

**Modes of Subducting Slab Motion and
Deformations:
Insights from Analogue and Numerical Models**

**Thesis submitted towards the partial fulfillment
of M.Sc. Final Examination in Applied Geology,
Jadavpur University**

**By
Rupsa Ray**

Registration no: 128246 of 2014-15

Exam Roll No: MGEO194009

Class Roll no: 001720402008

Department of Geological Sciences


Jadavpur University

Kolkata-700032

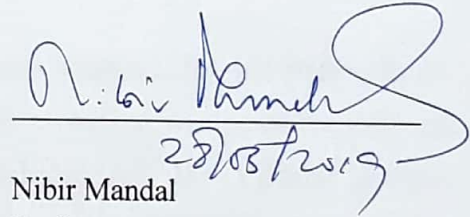
2019



This is to certify that Smt. Rupsa Ray has worked under my guidance and completed her thesis entitled **“Modes of Subducting Slab Motion and Deformations: Insights from analogue and numerical models”** in the Department of Geological Sciences, Jadavpur University. This thesis is being submitted towards the partial fulfillment of M.Sc. course in Applied Geology of Jadavpur University in the year 2019.


30/05/2019

Head of the Department,
Department of Geological Sciences
Jadavpur University
Kolkata
Head
Department of Geological Sciences
Jadavpur University
Kolkata-700032


28/05/2019

Nibir Mandal
Professor
Department of Geological Sciences
Jadavpur University, Kolkata

NIBIR MANDAL
Professor
Dept. of Geological Sciences
Jadavpur University
Kolkata - 700 032

ACKNOWLEDGEMENT

It has been a fruitful experience working on this dissertation topic at the Department of Geological Sciences, Jadavpur University, Kolkata, for the last two years of my Master Degree. I would like to take this golden opportunity to thank all those without whom my thesis, “Modes of Subducting Slab Motion and Deformation: Insights from Analogue and Numerical Models”, would not have taken its present shape.

I am extremely obliged to Jadavpur University for including this thesis program in the Masters curriculum, which builds a knack for research in the minds of young students, right from their formative years.

I express deep gratitude to my guide Dr. Nibir Mandal, Professor, Department of Geological Sciences, Jadavpur University, Kolkata, for his constant supervision and encouragement, during the course of dissertation. It was only his undying perseverance and support which helped me achieve my present status of work.

I am indeed grateful to Dr. Sanjoy Sanyal, Head of the Department, Department of Geological Sciences, Jadavpur University, Kolkata, for his cooperation as well as the funding required during this tenure.

I would like to thank Mr. Ritabrata Dasgupta (Research Scholar), for his irreplaceable assistance, both during the conducting of the experiments as well as writing of the thesis. I also thank Mr. Manaska Mukhopadhyay (Research Scholar) and Mr. Uddalak Biswas (Research Scholar) for lending a helping hand with the photography of the different analogue models. Besides, I thank other research scholars Mr. Dip Ghosh, Mr. Joyjeet Sen, Mr. Nandan Roy, Mr. Giridas Maity and my classmate, Mr. Manjis Chanda for their valuable suggestions and help.

I acknowledge my best friend, Mr. Subhabrata Das, who had immensely helped me with the Corel files and modification of the images. I am indeed obliged to my friend Mr. Debayan Sengupta, for reviewing through the report. Also, I am indebted to my sisters Ms. Anwesha Roy and Ms. Bidisha Roy for editing my thesis work.

Lastly, I would like to thank my parents without whose love, my thesis, would not have been complete.

ABSTRACT

Understanding the mechanics of convergent plate margins, in form of lithospheric subduction is a key to the study of earth's geodynamic processes. The effects of different subduction parameters on the temporal evolution and subduction dynamics of a subducting slab is well manifested in the evolution of slab dip and radius of curvature. The dynamics of slab motion influences the deformation in the slab occurring in sub-slab mantle. The slab deformation is governed by the force balance between negative buoyancy force, resisting mantle force and the viscous dissipation of forces during bending. Apart from these, slab deformation gets enhanced due to interaction with the transition zone. When slab deformation becomes much more intense and vigorous compared to the mechanical strength of the subducting slab it may get detached. Slab detachment may occur due to multiple reasons such as: temporal paucity in convergence motion of the subducting slab, thermal weakening in the slab, and presence of weak zone in form of dead ridges or pre-deformed strain weakened slab lithology etc. The aim of this study is to evaluate the modes of slab motion and dynamics in terms of slab dip and curvature and to find the criticality of mode shift from slab deformation to detachment. Two principle types of scaled laboratory experiments were performed: *Type A*- Homogeneous Slab and *Type B*- Slab with pre-defined weak-zones. Type A experiment using homogeneous slab, exhibit gradual increase in slab dip and decrease in radius of curvature, with time. With progressive time steps, slab flattening in the transition zone produced a number of subsidiary slab dips with values lower than the primary one. However, the deformation pattern changes when a pre-defined weak zone is introduced in the system. The weak zone is varied with competent and incompetent type of material. For experiments with competent weak zone, the slab exhibits steady increase of dip and decrease radius of curvature until folding. After reaching the transition zone the slab experiences profuse folding. The folding localizes at the introduced weak zone with progression of subduction. The slab dip reduces at the instance of folding and increases afterwards. However, for experiments with incompetent weak zone the slab becomes steep and exhibit necking in the weak zone without any detachment at initial stages. At the instance of detachment the slab dip

decreases as the slab rebounds as a consequence of sudden reduction of negative buoyancy. Computational fluid dynamic (CFD) experiments were performed to evaluate different slab deformation modes. The experiments were conducted varying the ages of the subducting lithosphere and detachment was induced by paucity in convergence motion, without introducing any pre-defined weak zone within the slabs. Experiments reveal that slabs may get folded but not detached when the convergence rate is constant temporally and the slab is sufficiently young (≤ 60 Ma age). However, paucity in the convergence motion of an old (100 Ma) subducting slab results in slab detachment due to force partitioning between the pull and push component. From experiments it can be seen that the detachment is a continuous process which is accomplished by progressive necking of the slab. Moreover, numerical simulations reveal the essential criticality of negative buoyancy for detachment in form of slab age. From this study, it is evident that the process of slab detachment is guided by viscous necking. Detachment of subducting slab by necking and vanishing of slab pull force as a consequence is manifested in temporal evolution of parameters like reduction slab dip and radius of curvature.

CONTENTS

Chapter 1: Introduction.....	1-11
1.1 General description of plate tectonics	
1.2 Types of plate boundaries	
1.3 Architecture of subduction zones	
1.4 Subduction kinematics	
1.5 Slab detachment in subduction zones	
1.6 Outline of thesis work	
Chapter 2: Theory of subducting plate motion.....	12-33
2.1 Corner flow theory for predicting slab dip	
2.2 Review of theoretical studies on subduction curvatures	
2.3 Review of experimental models for subducting plate deformation	
Chapter 3: Laboratory set-up.....	34-45
3.1 Introductory note	
3.2 Concept of model scaling	
3.3 Model material	
3.4 Model design	
3.5 Physical variables	
3.6 Types of experiment	
Chapter 4: Subduction zones in analogue models.....	46-56
4.1 General description	
4.2 Subduction dip analysis	
4.3 Subducting plate curvature	
4.4 Subducting plate detachment	
4.5 Deformed slab geometry	
Chapter 5: Theory of fluid dynamic simulation.....	57-61
Chapter 6: Subduction zones in numerical models.....	62-68
Chapter 7: Summary and Conclusions.....	69-70
References.....	71-72

CHAPTER 1:

INTRODUCTION

1.1. General Description of Plate Tectonics

Plate tectonics is a global phenomenon that provides valuable insight into the surface manifestation of the internal energy of the earth, primarily mantle convection. Theory of plate tectonics explains the mechanisms by which earth's crust have been formed as well as how earth has been cooling down, since millions of years. It is a unifying model that attempts to explain ideas such as the origin of patterns of deformation in the crust, earthquake distribution, supercontinents formation and breakdown, and mid-oceanic ridges.

Two major premises of plate tectonics are:

- (1) The lithospheric plates (crust and the upper part of the mantle) behave as a strong, rigid substance resting on a weaker asthenosphere (comparatively plastic).
- (2) The lithosphere is segmented into numerous major and minor plates that are in motion with respect to one another and are continually changing in shape and size
(*Kent C. Condie, 2011*).

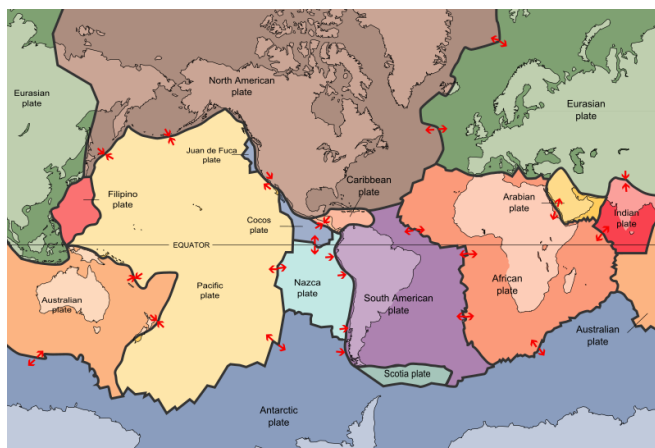


Figure 1.1: World map showing the distribution of various major and minor lithospheric plates.

These lithospheric plates are composed of either thinner oceanic lithosphere or thicker continental lithosphere. To accommodate the newly created lithosphere at the mid-oceanic ridge, oceanic plates return to the mantle along subduction zones, conserving the Earth's surface area nearly unchanged (*Kent C. Condie, 2011*). This prediction of plate tectonics is also referred to as the Conveyor Belt Principle.

Convection results in temperature induced density variations, giving rise to slow creeping motion in the mantle on a million year time scale. Plate movement is thought to be driven by a combination of the motion :

- (1) *Basal drag (friction)*: Plate motion driven by friction between the convection currents in the asthenosphere and the overlying lithosphere.
- (2) *Slab suction (gravity)*: Plate motion driven by local convection currents that exert a downward pull on plates in subduction zones at ocean trenches.

1.2 Types of Plate Boundaries

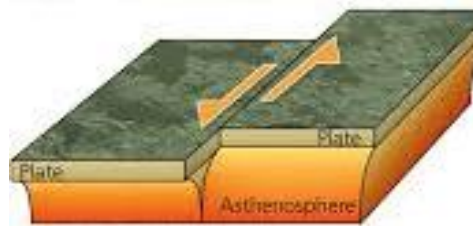
The Earth's lithosphere is broken into several plates of varying dimension whose boundaries are characterized by distinct tectonic movements. A range of geological phenomena, such as earthquakes, volcanic activities, orogeny and oceanic trench formation occur along these plate boundaries. Each type of these boundaries displays distinctive morphology, plate motion and tectonic activities.



Divergent plate boundary



Convergent plate boundary



Strike-slip plate boundary

Figure 1.2: Diagram demonstrating different types of plate boundaries

Three types of plate boundaries have been recognised:

(1) Divergent Boundaries

Divergent boundaries occur only at mid-ocean ridges and are the sites of creation of new lithosphere by seafloor spreading. These boundaries are characterized by extensional tectonics dominated by normal faulting and extensional earthquake focal mechanisms. Generally, a divergent plate boundary is approximately orthogonal to the plate separation or spreading direction, but this is not essential, and ridges with greater or lesser extents of obliquity are fairly common (*R.C. Searle, 2015*). Typical examples of divergent boundaries are the Atlantic Ridge, East Pacific Rise and the Indian Ocean ridge.

(2) Convergent Boundaries

Convergent plate boundaries occur at the deep-sea trenches and related 'subduction zones'. Areas of active mountain building on continents are zones of plate convergence, but are characterized by broad and almost continuous zones of deformation. This is partly because continental lithosphere is weaker and more easily deformed than oceanic lithosphere, and partly because it is less dense and so is not readily removed by subduction. Plate tectonics does not provide a very useful description of such broad continental convergence zones (*R.C. Searle, 2015*). Typical example is the Alpine-Himalayan zone.

(3) Transform fault Boundaries

Transform boundaries are those in which plates slide past one another with essentially no convergence or divergence; they thus conserve the areas of the adjacent plates. Because of this, they have the important property that they are exactly parallel to the direction of relative plate motion, and can be used for its estimation. Transform boundaries are characterized by strike-slip faulting and earthquakes with strike-slip mechanisms (*R.C. Searle, 2015*). A typical example is San Andreas Fault Zone, California, USA.

1.3 Architecture of Subduction Zone

A mature and stable subduction zone causes magmatic and tectonic phenomena in the overlying lithosphere, which can be recognized as "arc-trench complexes" (*Stern, 2002*). These complexes provide useful information on plate tectonics, even after subduction has ceased. They are divided into three components, namely, fore-arc, magmatic arc and back- arc.

(1) Fore-arc

Fore-arc basins lie in between the trench and the magmatic arc. These basins typically develop along continental margins and island arcs where oceanic plates are subducting beneath the overriding crust (*Noda, 2016*).

Convergent plate boundaries were initially divided into accretionary (AC) and non-accretionary (also includes erosional) types, depending on the transport of material between the plate boundaries, during fore-arc basin evolution .The AC type has evidences that the outer wedge was growing (widening or thickening) due to accretion of imbricated trench fill sediments at the toe of the outer wedge(frontal accretion) or accretion of stacked sediments beneath the outer or inner wedge (basal accretion or underplating). The non-AC type has margins with no evidence of accretion (true non-AC) and those with evidences of shrinking (thinning or narrowing) of the outer wedge, where mass wasting processes were dominant at the toe and subsidence occurred related with normal faults in the overriding plate (*Noda,2016*).

Secondly, each type was divided into compressional, neutral, and extensional types based on the strain regime in the basin. The compressional basins are characterized by thrusts and folds, especially in the seaward margins of them, and landward migration of the depo-centre. On the other hand, the extensional basins were subsided by crustal thinning, usually associated with normal faulting in the inner wedge, and seaward migration or stabilization of the depo-centre. The neutral type is intermediate one; most of which were associated with strike-slip faults due to oblique subduction (*Noda,2016*).

However, since fore-arc evolution is a long term process, these sub-basins have a tendency to transform from one type to another due to the action of plate tectonics.

(2) Magmatic arc

Where an oceanic plate is sinking beneath a less dense continental plate at a subduction zone, the region of raised elevation between the fore-arc and back-arc basins, where magma is rising, known as magmatic arcs. Magmatic arcs are linear arrays of point sources, caused by Rayleigh-Taylor instabilities in the mantle wedge above subduction zones (*Marsh, 1979*). This melt zone results when hydrous fluids released from subducted materials drastically lower the melting temperature of the overlying asthenospheric mantle (*Noda, 2016*).

(3) Back-arc

The back arc region lies behind the magmatic arc, and it can show a wide range of magmatic and tectonic styles, depending on strain class (*Jarrard, 1986*). Low strain arcs (strain classes 1 or 2) are associated with back-arc extension, whereas arcs with high strain (strain classes 6 or 7) may be associated with back arc folding and thrusting. Intermediate strain classes may be associated with a back arc region showing little or no tectonic or magmatic activity (*Noda, 2016*).

Active extension, rifting and seafloor spreading, characterize the back arc regions. Back arc spreading systems are remarkably similar to mid-ocean ridges. Fast spreading back arc basins have inflated ridge morphologies frequently underlain by geophysically imaginable axial magma chambers (*Turner et al., 1999*), while slow spreading back arc basins have axial rift morphology and occasionally expose mantle and lower crustal sections (*Hawkins et al., 1990; Stern et al., 1996; Ohara et al., 2002*). Hydrothermal vent fields are common along back arc basin spreading ridges, although the composition of fluids, deposits, and biota is distinctive.

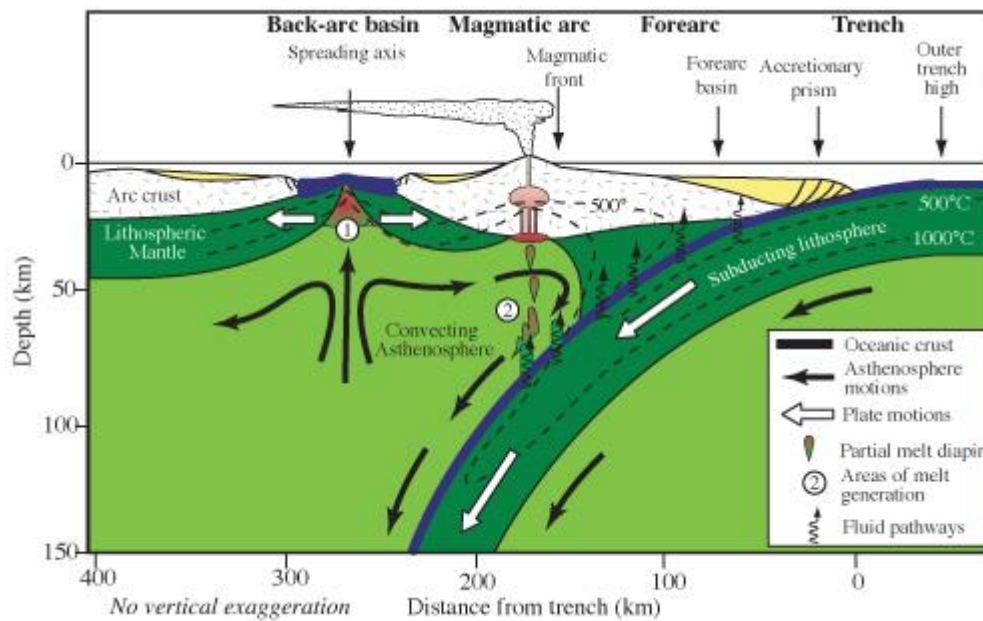


Figure 1.3: Schematic diagram showing the architecture of a Subduction zone.

1.4. Subduction Kinematics

The subduction process is a vital ingredient of plate tectonics (*Anderson, 1989, 2001; Stern, 2002; Conrad and Lithgow-Bertelloni, 2003*). Most of the oceanic lithosphere is recycled into the mantle, but also some continental lithosphere can subduct (*Ampferer, 1906; Ranalli et al., 2000; Hermann, 2002*). There still are doubts on the initiation of the subduction process (*Spence, 1987; Niu et al., 2003*), but once activated, it may work for several tens of million years. Subduction zones have a related accretionary prism or orogen, a subduction hinge that can migrate (*Garfunkel et al., 1986*), and a large variety of geophysical, magmatological and geological signatures (*Isacks and Molnar, 1971; Jarrard, 1986; Royden and Burchfiel, 1989; Tatsumi and Eggin, 1995; Hacker et al., 2003; Carminati et al., 2004; Ernst, 2005*).

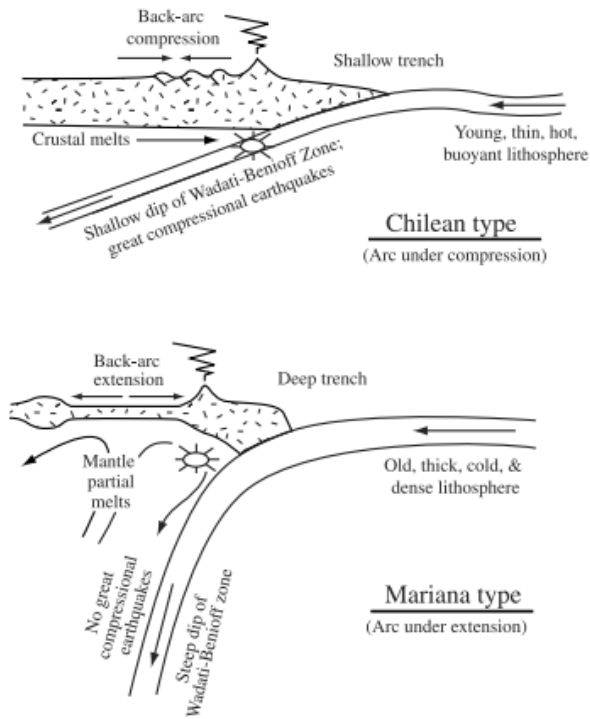


Figure 1.5: End-member types of subduction zones, based on the age of lithosphere being subducted (modified after *Uyeda and Kanamori* [1979]).

Subduction zones and related orogens show significant differences as a function of their polarity. They can be of two types- one, Chilean type, exhibiting a low dip and another, high dip Mariana type, showing high dip. Such cases are prevalent in nature and we get evidences from Japan Trench (dip amount 10°) and Central Peru Trench (dip amount 44°). This difference in dip amount is highly dependent on the horizontal mantle flow. This is a generally accepted idea and is used for explaining various important subduction dynamics. “West”-directed subduction zones are on average steeper ($\sim 65^\circ$) than “East”-directed ($\sim 27^\circ$). Also, a ‘Westerly’ directed net rotation of the lithosphere has been directed relative to the mantle in the hotspot reference frame. Thus the presence of an ‘Easterly’-directed horizontal mantle flow could essentially explain the subduction asymmetry, favouring steepening or shallowing of the subduction dip angle (*E.Ficini et.al, 2017*).

W-directed slabs are generally very steep (up to 90°) and deep, they have co-genetic back arc basin; the related single-vergent accretionary prism has low elevation, it is mostly composed of shallow rocks, and has a frontal deep trench or foredeep (*Doglioni et al., 1999*). The E- or NE-directed subduction zones are less inclined ($30\text{--}60^\circ$), and seismicity generally

dies at about 300 km, apart some deeper clusters close to the upper-lower mantle transition (*Omori et al., 2004*). The related orogens have high morphological and structural elevation, wide outcrops of basement rocks, and two shallower trenches or foredeeps at the fronts of the double-vergent belt, i.e., the forebelt and the retrobelt. These differences can be ascribed to shallower upper-crustal decollments typical of W-directed subduction zones with respect to the deeper lithospheric-rooted decollements occurring along E- and NE-directed subduction zones.

1.5 Slab Detachment in Subduction Zones and their Geological Consequences

In plate tectonics, slab detachment may occur during continent-continent or arc-continent collisions. Here, primarily we would be dealing with an ocean-continent subduction set-up. When the continental margin of the subducting plate reaches the oceanic trench of the subduction zone, the more buoyant continental crust will, in normal circumstances experience only a limited amount of subduction into the asthenosphere. The slab pull forces will, however, still be present and this normally leads to the breaking off or detachment of the descending slab from the rest of the plate (*Van Hunen J.; Allen M.B., 2011*). The isostatic response to the detachment of the downgoing slab is rapid uplift. Slab detachment is also followed by the upwelling of relatively hot asthenosphere to fill the gap created, leading in many cases to magmatism (*Whalen J.B.; McNicoll V.J.; vanStaal C.R.; Lissenberg C.J.; Longstaffe F.J.; Jenner G.A.; van Breeman O. 2006*). The propagation of the detachment will be accompanied by lateral migration of both the associated uplift and the magmatism (*Wortel M.J.R.; Spakman W. 2000*).

A model proposed that oceanic lithosphere detaches from continental lithosphere during continental collision (slab breakoff), allowing an explanation of syn- to post-collisional magmatism and metamorphism. Continental collisions are preceded by subduction of dense oceanic lithosphere, and followed by attempted subduction of buoyant continental lithosphere. This situation of opposing buoyancy forces leads to extensional deformation in the subducted slab. A narrow rifting mode of deformation will result if there is strain localization.

The plausibility of this process was assessed by quantitatively evaluating an upper bound for the strength of the lithosphere, and it has been compared with the change in buoyancy force during continental subduction. Whether break off will occur, and the depth at which it will occur, is a strong function of temperature and hence the subduction velocity. For a subduction velocity of 1 cm/yr breakoff could occur at depths of between 50 and 120 km, while at higher velocities it is still likely to occur, but at deeper depths.

As a result of the rifting during break off, the asthenosphere upwells into the narrow rift, and following break off, it impinges on the mechanical lithosphere of the overriding plate. The resulting conducted thermal perturbation leads to melting of the metasomatised overriding mantle lithosphere, producing basaltic magmatism that leads to granitic magmatism in the crust. Dry asthenospheric mantle will melt only if break off occurs at a depth shallower than ca. 50 km. Break off removes the force at the down dip side of the continental crust, while the enhanced heating leads to a reduction of the strength of the underlying crust. Both effects facilitate the freeing of buoyant crustal sheets which can then rise towards the surface, leading to the rapid exhumation of eclogite facies continental crust. The cessation of subduction and replacement of the cold oceanic lithosphere by asthenosphere leads to rapid uplift of the orogen.

1.6 Outline of Thesis Work

Analogues as well as numerical modeling were carried out to investigate the behavior of lithospheric plate, when subjected to subduction. Critical parameters like slab dip and slab curvature were studied in order to determine the processes guiding it and the existence of weak zone in the lithospheric plate.

For our convenience, we have divided the experiments into two categories- one, without weak zone and another, with weak zone, i.e., Type 1 and Type 2. Further, Type 2 experiments were divided into two more categories, i.e., Type 2A, with competent weak-zone and Type 2B with incompetent weak-zone.

Observations were documented based on the slab geometry, deformation, slab dip and curvature. The aim is to categorize the experimental observations based on different modes of slab deformation (e.g., slab folding or detachment).

CHAPTER 2:

THEORY OF SUBDUCTING PLATE MOTION

The basic notion of plate tectonics is that the plates are in constant motion and this motion is a surface manifestation of the deep seated energy in the mantle convection. Other processes such as trench migration or plate rheology have little effect on the angle of subduction (the angle of subducting plate with the Earth surface usually taken as horizontal), instead of these processes the critical factor affecting the subduction is the negative buoyancy of the subducting plate itself (*Stevenson and Turner, 1977*). The subduction plate motion is not only about the vertical sinking of the plate but also includes the horizontal movement of the plate along with the trench movement. Thus, the negative subducting plate buoyancy does not only affect the angle of subduction but also affect its curvature (*Capitanio and Morra, 2011*). The major consequences of subduction are slab (subducting plate) buckling and slab detachment. These have a major role to deforming the subducting plate and may results into different folding pattern (*Schellart, 2011*) and subduction reversal (*Boutelier and Cruden, 2016*) respectively.

2.1 Corner Flow Theory

The “Corner Flow” is a laminar fluid dynamical model which states that the materials are driven into the mantle by the subducting plate but some of the crustal material are ejected back to the surface along the slab depending on the angle of subduction and are never taken into the deeper mantle level once they are exhumed on the surface. It takes into account of the torques acting on the subducting plate which are themselves function of the subducting plate

length, depth of subduction, subducting plate rigidity and the fractures existing in the plate. The theory assumes that the mantle is of homogeneous viscosity and convectively neutral with the subducting slab be rigid and moving at a steady speed.

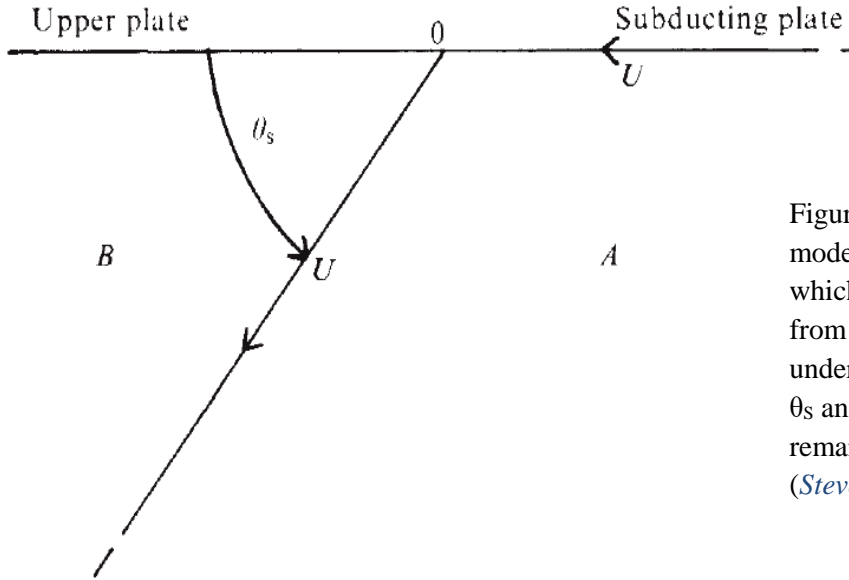


Figure 2.1: Two-dimensional model for a subduction zone in which materials are transported from the ridge to 0 where it undergoes subduction at an angle θ_s and velocity U . The upper plate remains rigid and stationary (Stevenson and Turner, 1977).

For thin and infinitely long subducting plate, the hydrodynamic contribution to the pressure in region A and B are given as follows (Stevenson and Turner, 1977):-

$$P_A(\theta) = \frac{2\mu U [\sin \theta - \sin (\theta - \theta_s)]}{r[(\pi - \theta_s) + \sin \theta_s]} \quad (1)$$

$$P_B(\theta) = \frac{-2\mu U [\sin \theta \sin \theta_s + \theta_s \sin (\theta_s - \theta)]}{r[\theta_s^2 - \sin^2 \theta_s]} \quad (2)$$

There are minor modifications induced in these pressure regimes by the back-arc spreading with associated diapiric upwelling of magma and the shearing heat in the edge of subduction. These modifications have minimal effect on the torques associated with the subduction. As the pressure on the A region is more than the pressure on the B region, this pressure difference always tries to reduce the angle of subduction. The torque about the point of subduction (0) due to this suction is given by (*Stevenson and Turner, 1977*) :-

$$T_H = \int_0^L [P_A(\theta_s) - P_B(\theta_s)] r dr$$

$$= 2\mu UL \left[\frac{\sin \theta_s}{(\pi - \theta_s) + \sin \theta_s} + \frac{\sin^2 \theta_s}{\theta_s^2 - \sin^2 \theta_s} \right]$$

Where L is the length of subducting plate and other symbol indicate the same as above. This torque is balanced by the torque produced from the negative buoyancy of the subducting plate which is denoted as T_G . If $\Delta\rho(r)$ is the density difference between the plate and the mantle with 'h' being the plate thickness, then the torque T_G (*Stevenson and Turner, 1977*):-

$$T_G = \int_0^L \Delta \rho (r) g h r \cos \theta_s dr$$

$$= \frac{1}{2} b L^2 \cos \theta_s$$

$$b = g h \int_0^1 \Delta \rho (x) dx$$

Where “ $x = r^2/L^2$ ”, “ g ” is acceleration due to gravity and “ b ” is negative buoyancy per unit slab area. The incorporation of “ h ” in definition of “ b ” indicates that the subduction is aided by the density contrast or by thickening of subducting plate. The solution for $T_G = T_H$ is given graphically for $b \geq b_c$; for $b > b_c$ there are two solution possible where the larger θ_s is stable as it produces restoring torque against any small perturbation. The model predicts that the stable angle of subduction should be greater than 60° but smaller angles are also observed which could be attributed to the finite torque required to bend the plate or the hydrodynamic pressure on the leading edge of the subducting plate.

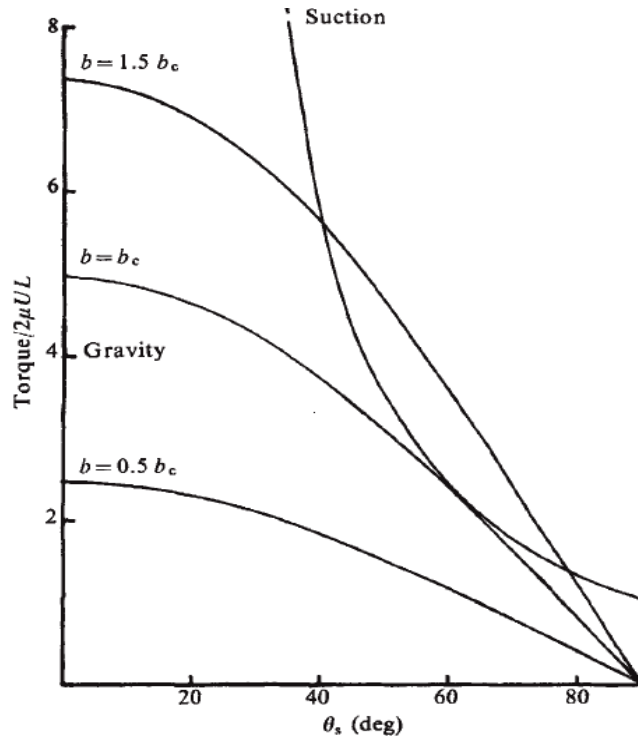


Figure 2.2: Torque (in units of $2\mu UL$) as a function of subducting angle. For $b < b_c$ there is no solution for $T_H = T_G$ but for $b = b_c$ there is a unique solution for $b = b_c$ whereas there are two solution for $b > b_c$ (Stevenson and Turner, 1977).

The model is over-simplified and not complete as it does not provide light on the initiation of the subduction and does not take into account the role played by the viscous drag and the ridge push, but at the same time provides clue about the negative buoyancy of the subducting plate resulting from cooling and thickening of the plate. The size of the plate subducting depends on the time taken to achieve critical negative buoyancy and it depends upon the geothermal heat fluxes which has varied through geological time period and thus, it provides clue to the fact that the plate tectonics in the Pre-Cambrian was much different from present.

2.2 Subducting Slab Curvature

The bending of the subducting plate is primarily a resultant of the vertical forces causing sinking of the subducting plate and the resistance due to the plate stiffness and rheology. But there are many intermittent forces that may have a local effect on the subducting plate which may include the suction force by mantle wedge and the far-field forces. The far-field stress varies with the dip

and the radii of the curvature of the slab depending on the factors that are creating those fields but are independent of the factors affecting subducting plate dynamics such as plate velocity or rigidity or thickness. On the other hand the suction force is dependent on the slab size and the geothermal flux; the negative buoyancy primarily depends on the size and the density of the plate. The slab buoyancy is the major cause for vertical downward movement of the subducting plate but other than that it has also been observed that at shallow mantle depths, the suction force works to uplift the subducting plate which provides torque against the negative buoyancy of the plate causing a decrease in the curvature of the plate than alone done by the negative buoyancy, including the far-field forces which are in general acting along the negative buoyancy causing an increase in the angle of subduction and an increase in the curvature of the bending of the plate. In a dynamic system, the rate of plate advance, dip and radius of the bending are correlated.

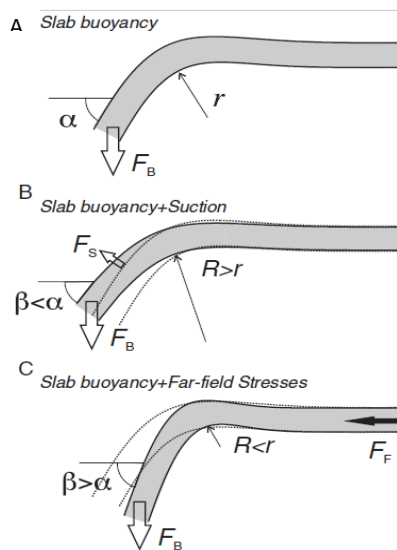


Figure 2.3: Sketch of the force balance around the bending lithosphere. (A) Slab buoyancy driven bending, (B) slab buoyancy and suction force, and (C) slab buoyancy and far-field force. The effect of the suction decreases the curvature thus increasing the radius and making the slab dip is shallower. Far-field forces increase the curvature at the trench and thus the radius is smaller and slab dips eventually

2.2.1 Role of Slab Buoyancy:

In general, it is found that there is an increase in curvature of the bending of the subducting plate with increase in plate buoyancy for constant viscosity and density difference between the plate and mantle whereas the slab dip decreases with increase in plate buoyancy.

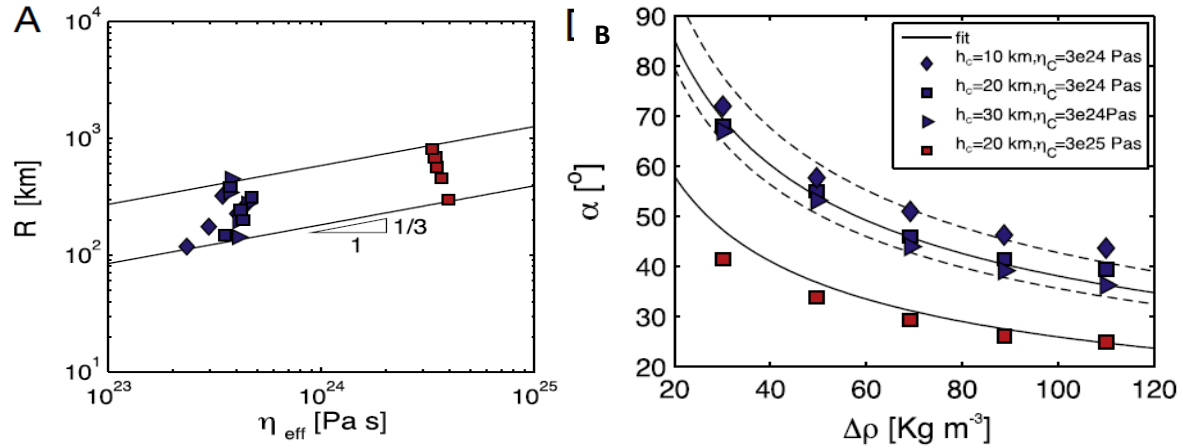


Figure 2.4: (A) Radii versus the effective viscosity; (B) Dips versus density difference ($\Delta\rho$) for the basic models, i.e. those driven solely by the slab buoyancy; h_c -stiff core thickness and η_c - stiff core viscosity of the lithospheric plate. Solid lines are for the proposed fit, dashed lines include the term h_c/h

2.2.2 Role of Far-Field Stresses:

Far-field stresses propagate from the bottom and the margins of the subducting plate to the trench. The asthenospheric drag (which is the resultant of the viscosity difference between the plate and mantle) resists the propagation of force, thus net push force increases with a decrease in asthenospheric drag. An equal viscosity for asthenosphere and mantle causes an increase in the dips and radii of the plate, whereas they tend to have smaller radii and steeper dips for smaller

differences. The lower asthenospheric drag amplifies the trend between asthenospheric drag and mantle drag where the mantle drag is as large as 100 times of the asthenospheric drag.

2.2.3 Role of Suction Force:

The suction force increases the bending radius twice than its value. This is due to the fact that the suction force is counteractive to the bending moment, resulting in a smaller curvature and subsequently larger radius. However this only affects the radius, whereas the dip does seem to remain same as in non-suction condition. An increase in curvature radius due to the suction force does not affect the plate velocity, since the deep dip variations are almost negligible.

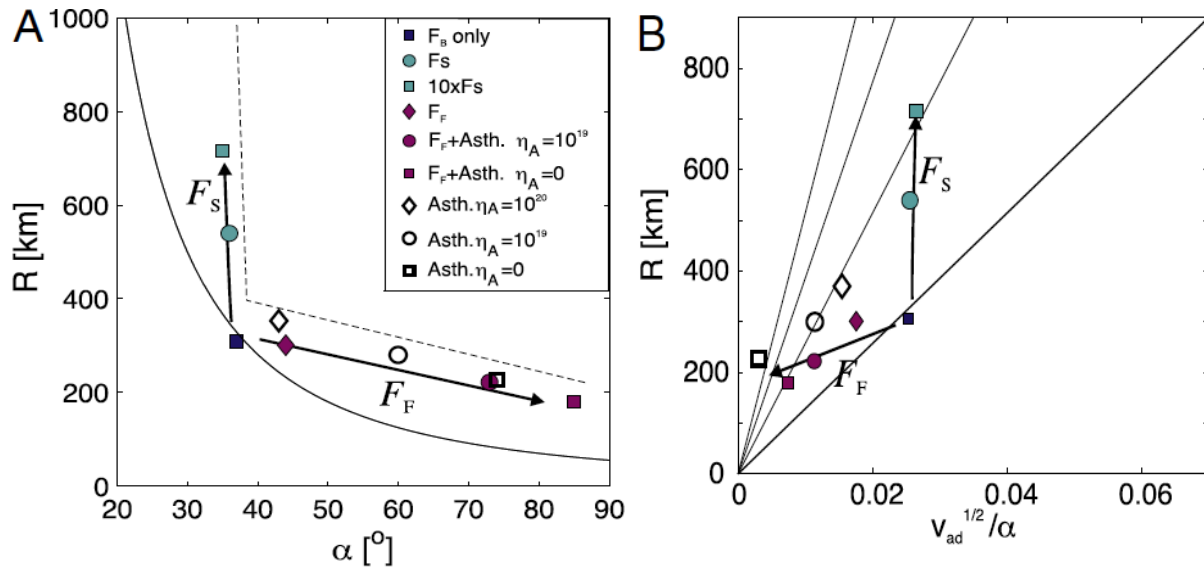


Figure 2.5: (A) Comparison of radius versus dip of models with suction and far-field stresses against models driven solely by slab buoyancy. The radii are up to two times larger when the largest suction is included; variable far-field forces induce tighter radii and larger dips. Solid lines are for the proposed fit, dashed lines include the term h_c/h where h_c -stiff core thickness and h - total subduction plate thickness; (B) Radii versus square root of the plate advance velocities (V_{ad}) divided by the dips (α). The suction force increases the radius up to two-fold, although it does not alter the dip or the plate velocity. F_{ar} -field stresses have a minor impact on radii, instead of having a more fundamental impact on the dips and the velocities. η_A -asthenospheric viscosity, F_F - Far-field force, F_S - Suction force (*Capitanio and Morra, 2011*).

2.3 Subducting Slab Deformation:

The subducting slabs undergo many changes and among them two phenomena which are wide spread and have a regional scale effect are as follows:

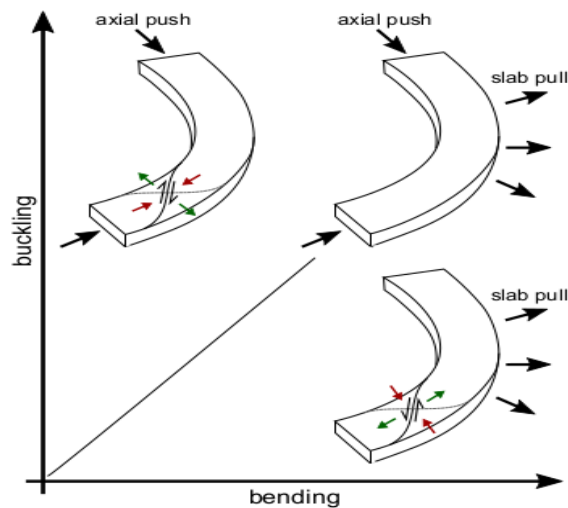


Figure 2.6: Dominant mechanisms of deformation.

- (1) *Subducting slab buckling*: Buckling is the active folding mechanism indicative of Layer-parallel shortening (LPS), it involves competency contrast and the more competent layer experiences an outer extensional zone and an inner compressional zone ([Schellart, 2011](#)). The trench migration, viscosity contrast and the angle of subduction plays pivotal role in this process ([Schellart, 2011](#); [Lee and King, 2011](#)).
- (2) *Slab detachment*: Detachment of slab means breaking off a portion of subducting plate beneath a convergent margin. This may lead to the culmination of the subduction or reversal of subduction polarity. Many factors are involved in the slab detachment process and of them few important processes are rigidity of slab, increase in temperature of slab ([Boutelier and Cruden, 2016](#)) and mineralogical phase change that may cause a shallower slab break-off rather than a deeper one ([Duretz et al., 2010](#)).

2.3.1 Slab Buckling

The geometry of subducted slabs interacting with the transition zone is decided by the partitioning factor which includes subduction velocity ($V_{S\perp}$) at or near to the surface into two components, which includes subducting plate motion component ($V_{SP\perp}$) and trench migration component ($V_{T\perp}$). Geodynamic models of progressive subduction suggest that there is an existence of five distinct slab geometries with their associated buckling fold types characterised by the ratio of ($V_{SP\perp}/V_{P\perp}$) which includes slab draping ($V_{SP\perp}/V_{P\perp} \leq 0.5$), slab draping with recumbent folds ($0.5 < V_{SP\perp}/V_{P\perp} < \sim 0.8$), slab piling ($\sim 0.8 \leq V_{SP\perp}/V_{P\perp} \leq \sim 1.2$), slab roll-over with recumbent folds ($\sim 1.2 < V_{SP\perp}/V_{P\perp} < \sim 1.5$) and slab roll-over ($V_{SP\perp}/V_{P\perp} \geq \sim 1.5$). Different physical parameters influence subducting plate buckling which includes mantle stratification, slab/upper mantle viscosity ratio and model boundary condition (*Schellart, 2011*). A buckling can happen in presence of stress field associated with the subduction process for e.g. there is a strong correlation between the slab dip and the stress in the back-arc environment; shallower dips correlate with back-arc shortening (Aleutians, Japan-Kuril (JK) and Andes) while steeper dips correlate with back-arc extension (Mariana, Sumatra and Tonga–Kermadec). Other contributing factors to this stress field are such as convergence rate and slab age and the slab dips but they are seemingly to be more random than just putting a strong correlation. The state of back-arc stress may change with time; the back-arc basin which is experiencing temporal shortening which are expressed as thrusts may be followed by extension which is expressed as sediment deposition in the basins formed by this process (*Lee and King, 2011*). The slab buckles when the viscosity increases across the 660 km discontinuity is larger than 10^{20} Pa.s. The slab with lower viscosity subducts with negligible lateral slab deformation (no slab buckling) in the lower mantle. As we increase the viscosity across the 660 km discontinuity, the viscosity increase acts a barrier which slows down slab as it descends in the

lower mantle, and large lateral slab deformation (slab buckling) develops. Also it has been observed that fast subducting slab without buckling develops vigorous convection cells around the subducting slab and throughout the whole mantle; the upper and lower mantles are strongly coupled. In contrast to the experiments using smaller viscosity increase, the experiments using larger viscosity increase show fairly retarded slab penetration into the lower mantle. Thus, much weaker convection cells and slower convection develop in the mantle. Small-scale convection cells consisting of upwelling and downwelling vigorously develop between the lithosphere and the 660 km discontinuity. The periodic steepening and shallowing slab during the steady-state slab buckling phase can be related to the scattered slab dip. When periodic slab buckling develops, dynamic subduction history can be broken into three phases; initial unstable subduction with very fast subduction, a steady-state slab buckling resulting in periodic variations in the convergence rate of the incoming plate, and unbuckling of the stacked slab as the deep subducting slab enters the low viscosity CMB and slab detaches from the plate. The current and temporal stress environment and its distribution in the back-arc is an expression of the varying slab dip due to slab buckling; shallowing and steepening slab dips correspond to compressional and extensional back-arc, respectively (*Schellart, 2011; Lee and King, 2011*).

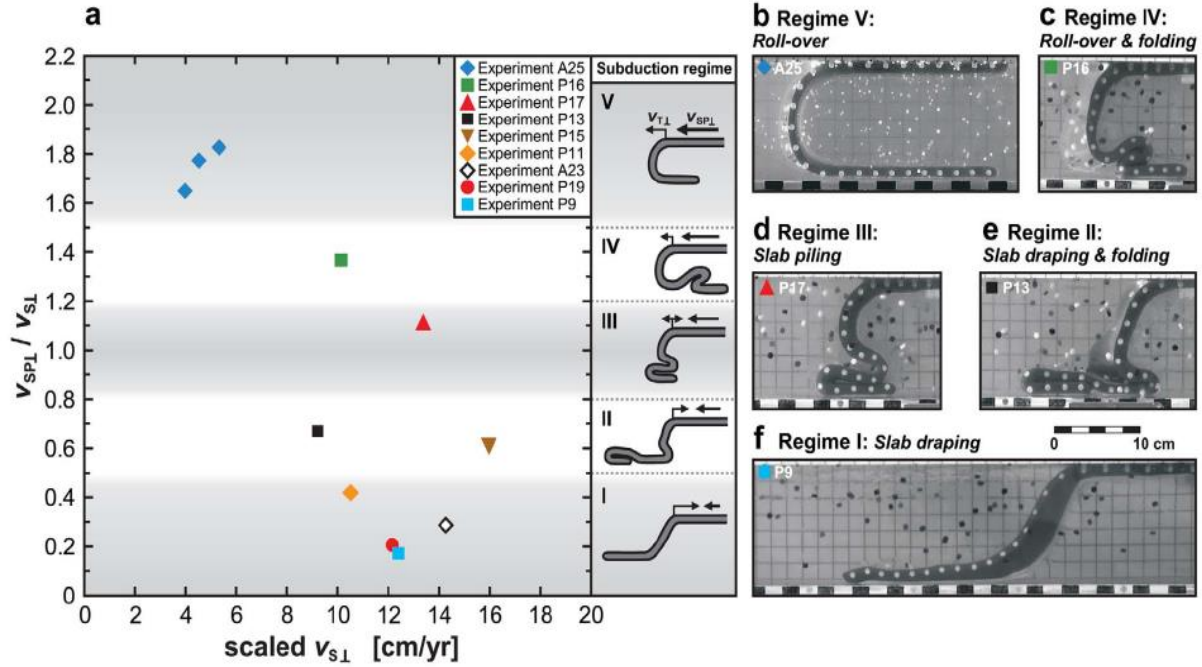


Figure 2.7: (a) Diagram illustrating average subduction velocity (V_{sL}) and subduction partitioning (V_{SPL}/V_{pL}) of nine three dimensional laboratory models of progressive subduction. Values for V_{SPL} and V_{TL} can be derived from Figure (a) through $V_{sL} = V_{SPL} + V_{TL}$. Also shown are the five main slab geometries observed that occur at distinct V_{SPL}/V_{pL} values, namely: slab draping (regime I, $V_{SPL}/V_{pL} \leq 0.5$), slab draping with recumbent folds (regime II, $0.5 < V_{SPL}/V_{pL} < \sim 0.8$), slab piling (regime III, $\sim 0.8 \leq V_{SPL}/V_{pL} \leq \sim 1.2$), slab roll-over with recumbent folds (regime IV, $\sim 1.2 < V_{SPL}/V_{pL} < \sim 1.5$), and slab roll-over (regime V, $\sim 1.5 \leq V_{SPL}/V_{pL}$). V_{SPL}/V_{pL} and V_{sL} have been averaged for $t' > 1$ (t' is the non-dimensional time where $t' = 1$ is the time when the slab tip first touches the bottom boundary of the box, i.e., the 660 km discontinuity). Averaging periods were distributed into four sets with same value for each set such that first set is (P9, P11, P13, A23 and A25), second set is (P16 and P19), thirs set is for (P17), and fourth is for (P15). (b–f) Side view photographs of five slab structure. Note that 1 cm in the models scales to ~ 50 km in nature. Also note that photos for each structure have been taken at a similar subduction stage with total amount of subduction of 32–36 cm (scaling to ~ 1600 – 1800 km) (Schellart, 2011).

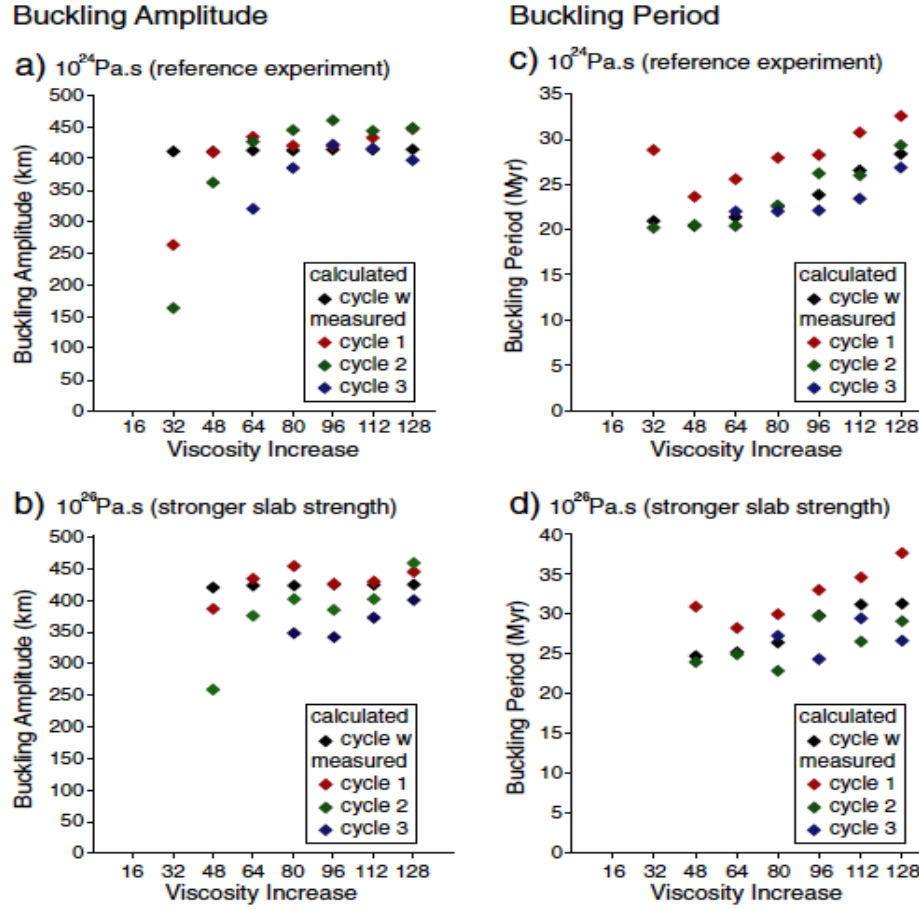


Figure 2.8: Buckling amplitudes (a and b) and periods (c and d) corresponding to the reference experiments and the experiments using the maximum slab viscosity of 1026 Pa.s, respectively. (a) Buckling amplitudes of the reference experiments varying viscosity increases across the 660 km discontinuity. Cycle w indicates the calculated buckling amplitude resulting from the scaling laws. Measured cycle 1, 2 and 3 (if there is 3rd cycle) are depicted with the cycle w. (b) Same as a except for the experiment using the maximum slab viscosity of 10^{26} Pa.s. (c) Buckling periods of the reference experiments varying viscosity increases across the 660 km discontinuity. Descriptions follow the same as a and b. (d) same with c except for the experiment using the maximum slab viscosity of 10^{26} Pa.s (*Lee and King, 2011*).

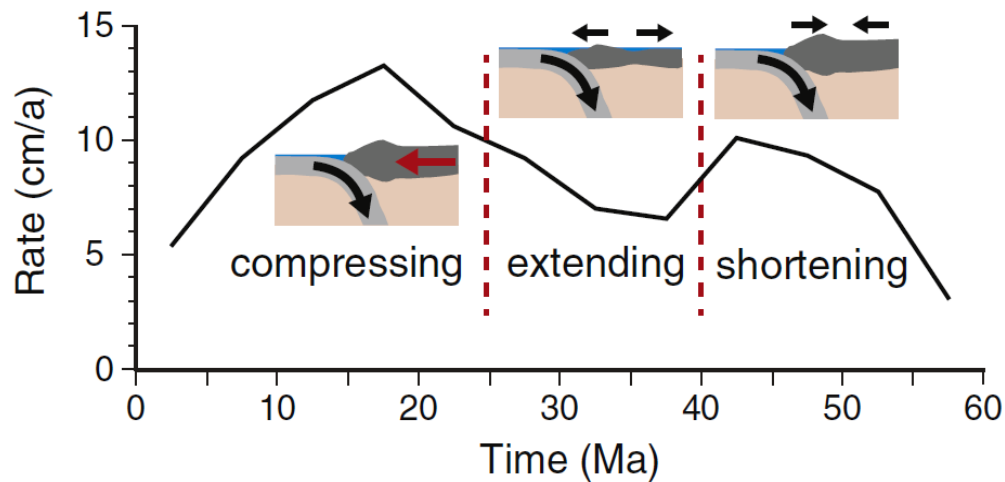


Figure 2.9: Evolution of Andean type back arc basin where there has been reversal of stress field from compression to extension and back to compression (*Lee and King, 2011*).

2.3.2 Slab detachment:

Slab detachment is generally associated with continental subduction. When positively buoyant continental lithosphere enters a subduction zone, down-dip tensile stress is generated in the previously subducted oceanic lithosphere, which can lead eventually to slab break-off. When slab break-off occurs, part of a subducted lithospheric plate detaches and sinks into the mantle. This process was first predicted as a geometrical necessity to account for observed reversals of subduction polarity in ancient orogens. Slab break-off has since been inferred from gaps in the distributions of earthquake hypocenters associated with subducted slabs and seismic tomography. Slab detachment is expected to cause a major change in the force balance in a subduction zone since the downward pull previously exerted by the subducted slab is removed. Consequently, slab break-off may cause important changes in plate kinematics and associated deformation. The reduction of subduction rate that accompanies subduction of buoyant crust also leads to a temperature increase in the subducted slab, thereby reducing its strength and accelerating break-off. The slab detachment is generally three-dimensional and diachronous, initiating in one location

and propagating horizontally along the plate boundary. The diachronous nature of slab detachment has been confirmed by three-dimensional analogue and numerical simulations. The diachronicity of the detachment implies that the tear must propagate along the plate boundary and there should be a characteristic signature that follows the propagating tear, which can be employed to reconstruct when and how slab detachment occurred. Also, there has been many statistical analysis of subduction zones reported which indicates that there are a number of slow subduction zones and therefore pre-collision convergence rate must be a variable parameter. The wide range of possible pre-collision convergence rates is illustrated by two end-members: the slow Alpine and the rapid Himalayan collisions. In subduction zones, the stress and tectonic regime in the overriding plate are mainly controlled by the normal and tangential stresses along the interplate zone which in turn can be affected by many other parameters. Mantle flow can also influence subduction dynamics and the stress in the plates via normal and tangential viscous stresses acting on the slab surface but they cannot be fully included with effects in the thermo-mechanical experiments, whereas the impact of the imposed subduction velocity on the slab strength and the associated evolution of the transmitted slab-pull force are major factors. The major effects of the convergence velocity lie in the fact that it is one of the main contributors to the magnitude of the horizontal pull force transmitted to both plates. A slow convergence rate results in a warmer and weaker slab, which can then detach when down-dip tension reaches a moderate threshold value. Slab detachment is preceded by rapid subsidence of the fore-arc basin associated with both trench normal and trench-parallel contraction. Following slab detachment, the fore-arc basin bounces upward due to elasticity and isostasy, and undergoes rapid but brief trench-parallel and trench-normal extension. An early slab detachment may occur during a collision that follows a period of protracted slow oceanic subduction because moderate down-dip tension generated by subduction

of continental crust may be sufficient to trigger early break-off of a thermally weakened slab. This scenario may correspond to the slow Alpine collision. The impact of convergence rate on temperature and strength of the subducting lithosphere also provides a mechanical explanation for slab detachment when a subduction zone becomes progressively more oblique and eventually evolves into a transform fault, as in the Aleutians or Sumatra-Andaman-Burma subduction zones. When subduction is highly oblique, the lithosphere is buried very slowly which is conducive to warming by the underlying mantle, resulting in a slab that is too weak to support significant down-dip tension (*Boutelier and Cruden, 2016*).

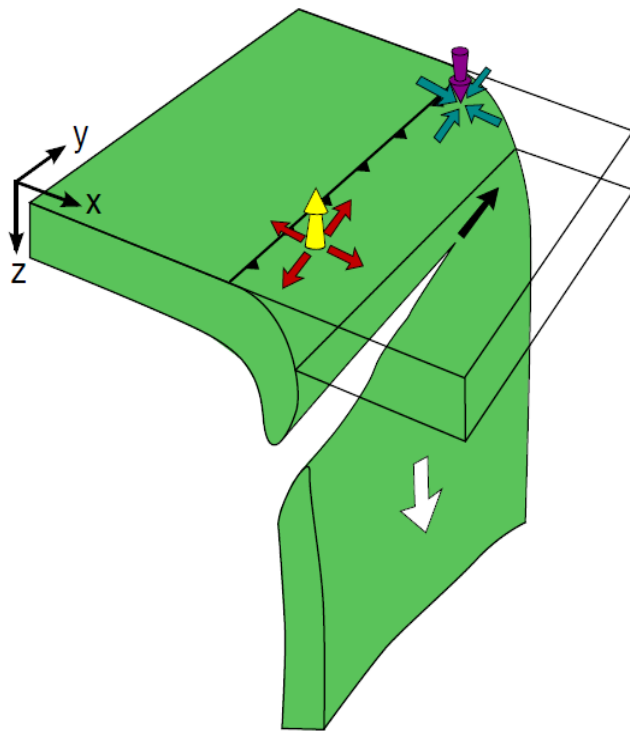


Figure 2.10: Sketch of propagating slab detachment with distribution of the induced surface deformation and vertical motions. Horizontal contraction and surface subsidence is generated ahead of the break-off tip, while horizontal extension and uplift follow

Other than the physical parameters affecting the breaking of the slab; there are some rheological parameters which may have a significant role to play in the slab break-off. They include: plasticity, viscous creep and Peierls creep. A strong correlation between average uplift rates and depth of break-off was observed in the experiments. Fast uplift rates can be expected in

the case of shallow slab detachment whereas deeper detachment provides slower uplift rates. Geological and geophysical studies suggest natural prototypes where uplift is related to slab break-off. The rheology of the lower crust plays a crucial role on the ability of the crust to support topography which has a strong lower continental crust of plagioclase rheology. For a weaker material (quartzite flow law) to simulate lower crust, comparable simulations would produce smoother topography and also display a broader orogen before and after slab detachment, this is because less crustal material is entrained in the subduction channel. This has the consequence to weaken the slab and therefore detachment occurs earlier and shallower than those which include a plagioclase lower crust. The weak lower crust induces a slower but broader topographic response on the lower plate. Slower rates may be related to the fact that the response is rather distributed (broader) on a weaker crust. Activation of Peierls mechanism by large extensional stresses in the cold core of the hanging slab is of first order importance for slab break-off modelling. It affects the timing and depth of break-off, along with a change in topography which is very different when the Peierls force is not present; in fact, Peierls force causes an earlier and shallower break-off. Old slabs can potentially contain a significant volume of metastable olivine on the prograde path. A buoyant olivine wedge has a tendency to slow down subduction, hence influencing the dynamics. It has also been observed that Plastic behaviour (Druker–Prager) is only important for shallow slab break affecting the crust. Peierls force appears to be a key mechanism for slab break-off dynamics. This mechanism plays an important in the mantle lithosphere for intermediate depth and slab break-off (*Duertz et al., 2010*). The slab detachment model is likely to be a fast geological process leading to (1) a partial or complete loss of the slab pull force and (2) the inflow of hot asthenosphere at the location of the detachment. The loss of slab pulls leads to force rebalancing in the orogen which can potentially trigger a wide range of dynamical effects. The slab

detachment model was consequently used for the explanation of high pressure and ultra-high pressure rock exhumation. But another parameter which has been worthy to be mentioned in this slab detachment process is the strong crust that is coupling at the Moho and remains coherent during subduction. It promotes deep subduction of the crust (180 km) and slab detachment. Exhumation occurs in coherent manners via subduction and thrusting. Slab detachment triggers the development of topography (>4.5 km) close to the suture. A contrasting style of collision occurs using a weak crustal rheology. Mechanical decoupling at the Moho promotes the extrusion of the crust, disabling slab detachment. Ongoing shortening leads to buckling of the crust and development of topography on the lower plate. Collisions involving rheologically layered crust allow decoupling at mid-crustal depths. This structure favours both the extrusion of upper crust and the subduction of the lower crust. Such collisions are successively affected by delamination and slab detachment. Topography develops together with the buoyant extrusion of crust onto the foreland and is further amplified by slab detachment (*Duretzand Gerya, 2012*).

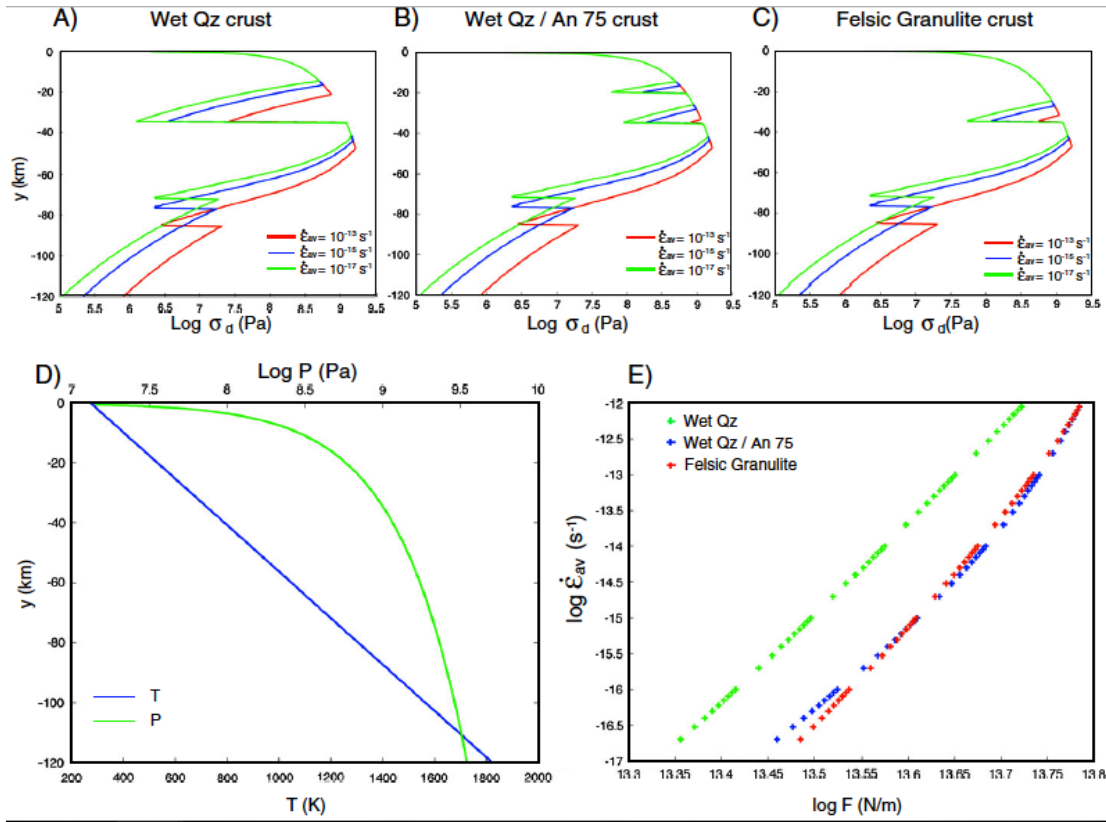


Figure 2.11: Example of rheological profiles for the different strength end-members for 3 different average strain rates. (A) Weak crust: quartzite rheology. (B) Layered quartzite/feldspar ($\dot{\epsilon}_{av}$ - Strain tensor rate, σ - Stress, F - Force per unit length) (Duretzand Gerya, 2012).

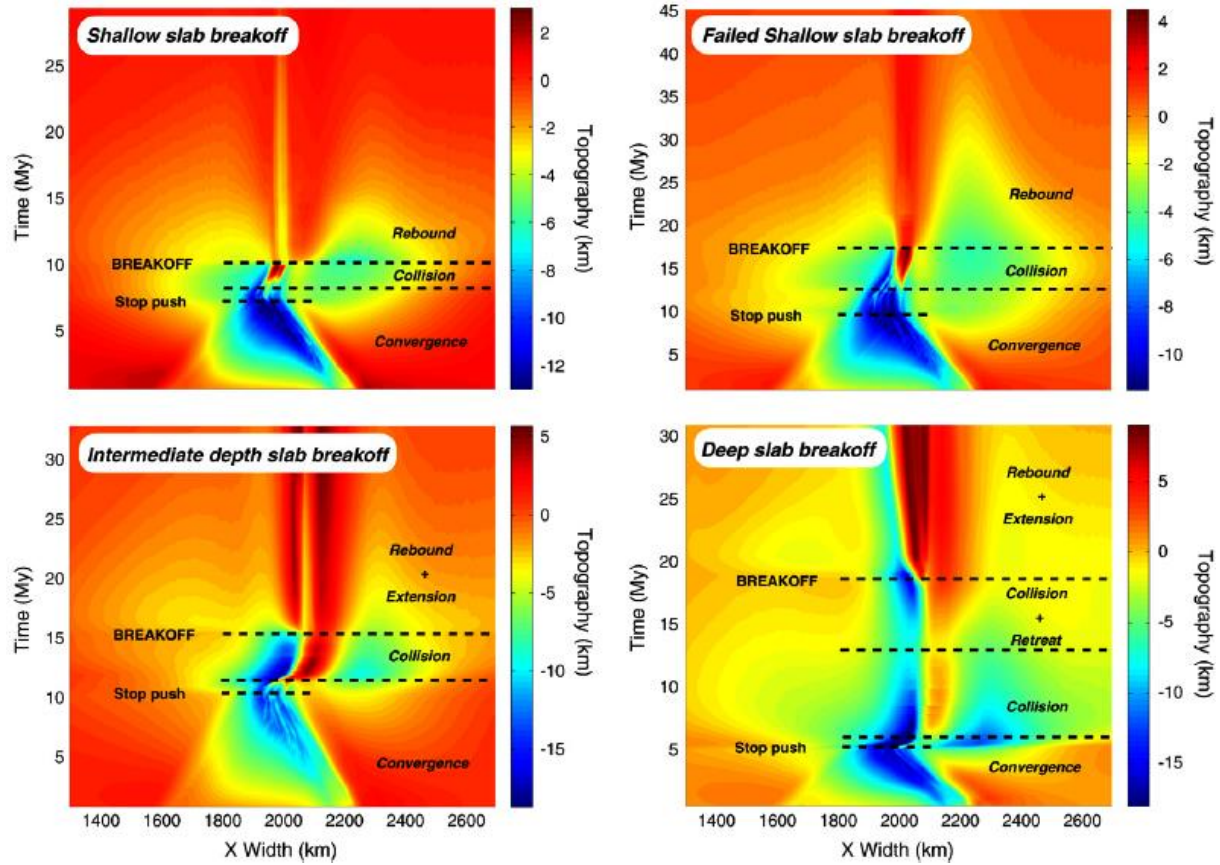


Figure 2.12: Topography evolution through time above the subduction–collision zone for each end-member. For each case, a sharp breakoff signal and subsequent uplift is observed. The overall topographic signal can be divided in time windows corresponding to different geodynamic stages (*Duertz et al., 2010*).

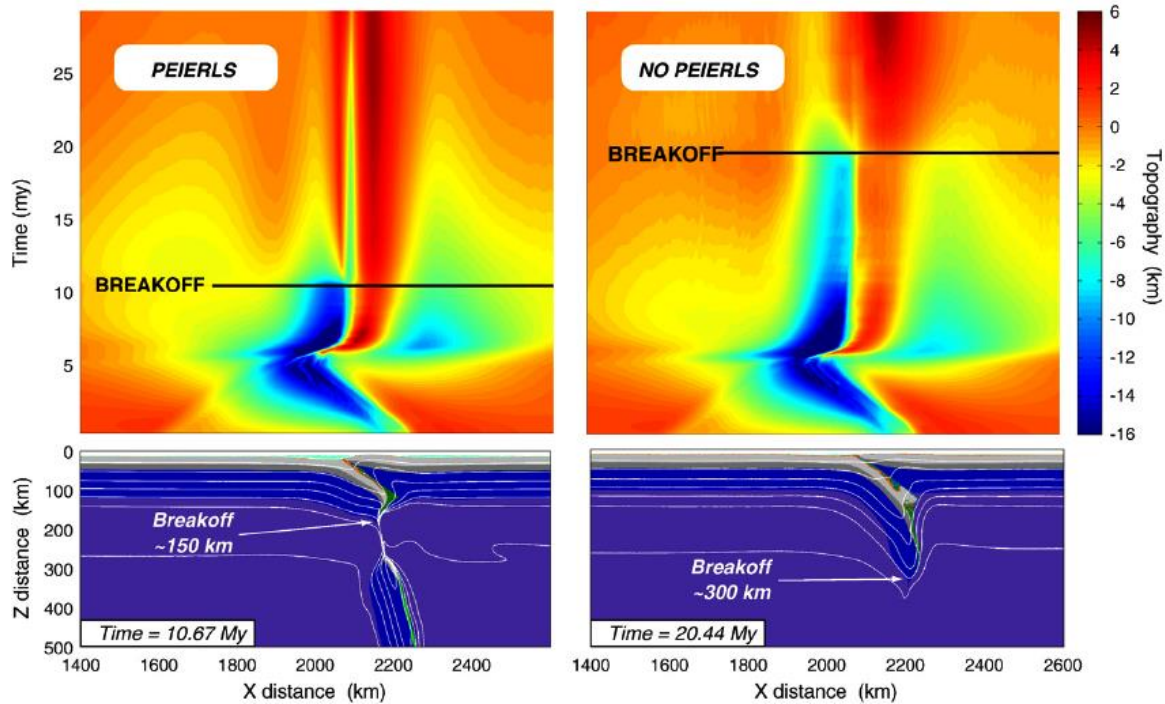


Figure 2.13: Comparison between models with and without Peierls mechanism. Parameters used in this setup are an oceanic lithosphere age of 40 My and initial total plate rate of 10 cm/yr. Origin of the z distance axis is the top of the box (including the 10 km thick air layer) (*Duertz et*

Also, it has been observed in coeval subduction of adjacent continental and oceanic lithospheres (SCO). This configuration yields to two-stage slab detachment during collision, topographic build-up and extrusion. The second setting considers a convergent margin, which is laterally limited by a transform boundary (STB) affected by a single slab detachment, little trench deformation, and moderately confined upper plate topography. During SCO, initially there is no along-trench variation and subduction of the oceanic basin leads to a laterally homogeneous subduction zone as well as the subsidence and back-arc extension of the upper plate triggering the opening of a back-arc basin material produces a subduction resistive force that will ultimately promote slab detachment after which continental collision takes place and crustal thickening

triggers lateral flow. This type of lateral extrusion internally affects the continental material but does not trigger rigid plate motion. Eventually the continental slab detaches after the necking of the continental slab, causing uplift of the lower plate. After detachment, the slab pull is reduced beneath the collision and is transferred along the trench affecting the adjacent oceanic slab. In the STB model, the initial stage of convergence triggers the development of subduction zone limited by the transform fault, as oceanic subduction develops, the upper plate subsides and is affected by back-arc extension. Continental collision initiates after sometime and the subducted continental margin undergoes necking under slab's negative buoyancy eventually leading to detachment. Slab thinning initiates at the slab's centre and migrates toward its edge. In the first stage, the topography induced by the collision is laterally limited by the transform fault and the signal of detachment is seen on the lower plate. The topography grows from the centre to the edge of the collision, witnessing the evolution of the. In the second stage, extrusion of topography overcomes the transform boundary and the thickened crustal material flows out of the collision zone. As slab pull is no more transmitted to the orogen and no kinematic push is prescribed, the lithospheric root becomes stalled and the slab sinks down to the 660 km boundary. In contrast with the SCO model, no effect of the mantle flow on the continental collision zone was observed as most of the flow induced by the slab's descent occurred around its edge (*Duertz et al., 2014*).

CHAPTER 3

LABORATORY SET-UP

3.1. Introductory Note

The geological phenomena occurring in nature, like that of mountain-building, subduction, volcanism etc are too complicated for us to study and analyse in reality. For this purpose we design mechanical models of deformation, to gain insight into these natural processes. This chapter encompasses both, scale models as well as numerical models, which together help us to understand the workings of nature (*Chapter-18, Scale Models And Quantitative Models Of Rock Deformation, Twiss, Moores; 2007*).

3.1.1. Scale Models

Scale models are actual physical models of parts of the Earth. The models are constructed with materials whose properties scale in such a way that their behaviour over short times and small distances reproduces the behavior of rocks over long periods of time and large distances (*Chapter-18, Scale Models And Quantitative Models Of Rock Deformation, Twiss, Moores; 2007*).

Knowledge of scaling theory to guides us in the selection of materials that could be used to model the Earth.

3.1.2. Mathematical Models

Mathematical models describe behavior in terms of sets of equations that define the mechanical behavior of particular materials (constitutive equations), the appropriate physical conservation laws that all systems must obey (in particular, the conservation of mass, momentum, angular momentum, and energy), and the specific physical constraints to which the body of material is subjected (the boundary and initial conditions) (*Chapter-18, Scale Models And Quantitative Models Of Rock Deformation, Twiss, Moores; 2007*).

3.2. Concept of Model Scaling

3.2.1 General Description

For many geologic situations, it is useful to make a scale model whose behavior on a scale of meters and hours is equivalent to what occurs in the Earth, the prototype system, on a scale of kilometers and millions of years (*Chapter-18, Scale Models And Quantitative Models Of Rock Deformation, Twiss, Moores; 2007*).

If the size of the body changes then other physical properties also change but is not proportional to the change of the size of the body. In order to investigate how various physical properties of a body changes with the change in the size of the body, a cube of lead is considered. It is then enlarged n diameters and the density are kept constant. Let n be successively 1,2,3,4,5 and so on. Then it is investigated in what manner the area, the volume, the mass, the weight and the pressure at the base of the cube change with different values of n .

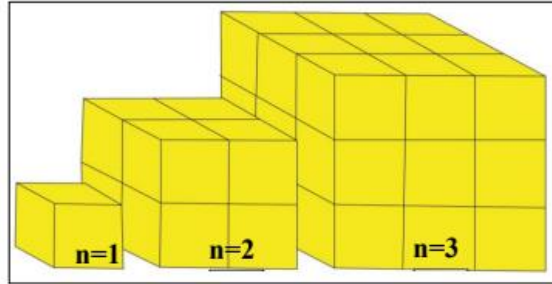


Figure 3.1: Change of magnitude of cube as length of sides are changed

When $n=1$, then each of the quantities are unity, that is, unit length, unit area, unit volume, unit mass, unit weight and unit pressure.

When $n=2$, length of the side=2, area=4, volume=8, mass=8, weight=8 and pressure at the base which is weight divided by area=2

When $n=3$, length of the side=3, area=9, volume=27, mass=27, weight=27 and the pressure at the base=3.

The table below shows upto $n=5$.

N	Length	Area	volume	Mass	Weight	Pressure
1	1	1	1	1	1	1
2	2	4	8	8	8	2
3	3	9	27	27	27	3
4	4	16	64	64	64	4
5	5	25	125	125	125	5

Table 3.1: Change in physical properties with change in size of the body. (*Hubbert, 1937*)

From this, it is understood that the area increases as square, the volume, the mass, the weight as cube and pressure at base of the cube as first power of the enlargement factor of a linear dimension of a cube, where gravity and density remain constant.

4.2.2 Degree of Similarity

(1) *Geometrical Similarity*- Two bodies are said to be geometrically similar and all the corresponding lengths are proportional and all the corresponding angles between two bodies are equal. If l_1 be the length in one of the bodies and l_2 be the corresponding length in other.

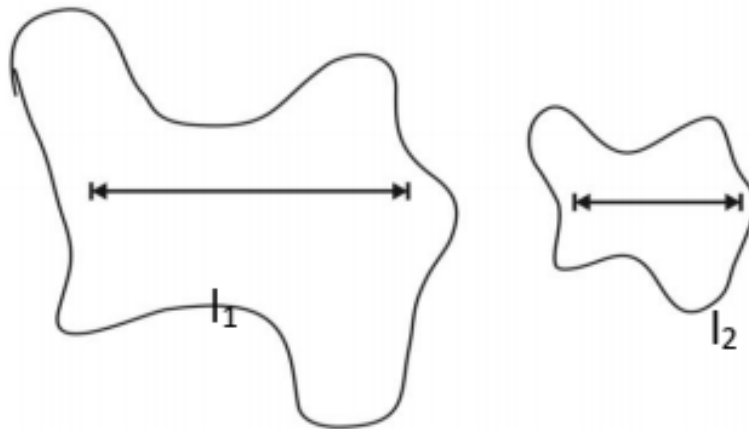


Figure 3.2: Two geometrically similar bodies (*Hubbert, 1937*).

Then,

$$l_2/l_1 = \lambda, \text{ or } l_2 = \lambda l_1$$

Where λ is the constant of proportionality of length of the two bodies.

If the first body is considered to be original and the second body is replica of the first made to scale, then the second body is the scale model for the former body. If reduction occurs, then it will be less than unity and if enlargement occurs then it will be greater than unity. λ is the model ratio of length. λ is a familiar map scale extended to three dimensions.

In two geometrically similar bodies, the ratio of areas of the corresponding bodies will be equal to the square of model ratio of length.

$$A_2/A_1=\lambda^2,$$

Where A_2 and A_1 are the corresponding areas of two bodies respectively. If the two areas are divided into similar grid works of n squares each, then,

$$l_2^2/l_1^2=\lambda^2,$$

Then for n such squares,

$$A_2/A_1=nl_2^2/nl_1^2=\lambda^2,$$

In two geometrically similar bodies, the ratio of corresponding volume for two bodies is,

$$V_2/V_1=nl_2^3/nl_1^3=\lambda^3,$$

(2) *Kinematic similarity*: If two geometrically similar bodies undergo geometrically similar changes in shape and position, or both, then they are said to be kinematically similar, provided the time for the given change in one body is proportional to that required for the corresponding change in the second body.

$$t_2/t_1=\tau,$$

Where t_1 is the time required for the transformation to occur in the original body and t_2 is the time required for the corresponding change in the model, and τ is the model ratio of time.

(3) *Similarity of velocity and acceleration*: If two bodies are kinematically similar then the velocities and accelerations of the corresponding bodies must be proportional.

$$v_2/v_1=\eta=l_2/t_2/l_1/t_1=\lambda/\tau^{-1}$$

Where v_1 and v_2 are velocities of the corresponding bodies and η is the model ratio of corresponding velocities.

For acceleration,

$$a_2/a_1=\gamma=l_2/t_2^2/l_1/t_1^2=\lambda/\tau^{-2}$$

Where γ is the model ratio of acceleration.

For angular velocities,

$$\omega_2/\omega_1=\Theta_2/t_2/\Theta_1/t_1=\Theta_2/\Theta_1.t_1/t_2,$$

Where, ω_1 and ω_2 are the angular velocities and Θ_1 and Θ_2 are the angles of rotation in the time t_1 and t_2 in the original and the model respectively.

But $\Theta_1 = \Theta_2$,

Therefore,

$$\omega_2/\omega_1=1/\tau = \tau^{-1}$$

(4) *Dynamic similarity*: While discussing the geometric and kinematic similarity, the relation between forms and motions have been described and here, mass is not considered. All the bodies contain mass. So the model needs to have mass distribution similar to that of the original one. If dm_1 is the mass of an element of volume dv_1 , in the original and dm_2 for corresponding element of volume, dv_2 , of the model such that the ratio is:

$$dm_2/dm_1=\mu,$$

And must hold for each point throughout the two bodies, μ being the model ratio of mass.

From model ratio of mass and length, the ratio of density can be obtained. The density can be defined by mass divided by volume. Model ratios of density δ is given by,

$$\delta= \rho_1/\rho_2=dm_2/dv_2/dm_1/dv_1=\mu\lambda^{-3},$$

And is constant throughout the two bodies.

3.3. Model Material

For the purpose of modelling, the following materials were used.



Low viscosity glucose syrup



High viscosity glucose syrup



Plasticine



**Poly Dimethyl Siloxane
(PDMS)**



Hand putty

Figure 3.3: Modelling materials.

- (1) Low viscosity glucose for upper mantle.
- (2) High viscosity glucose for lower mantle.
- (3) Plasticine for lithospheric plate.
- (4) PDMS (Poly Dimethyl Siloxane) for low viscosity contrast weak zone.
- (5) Hand putty for high viscosity contrast weak zone.

3.4. Model Design

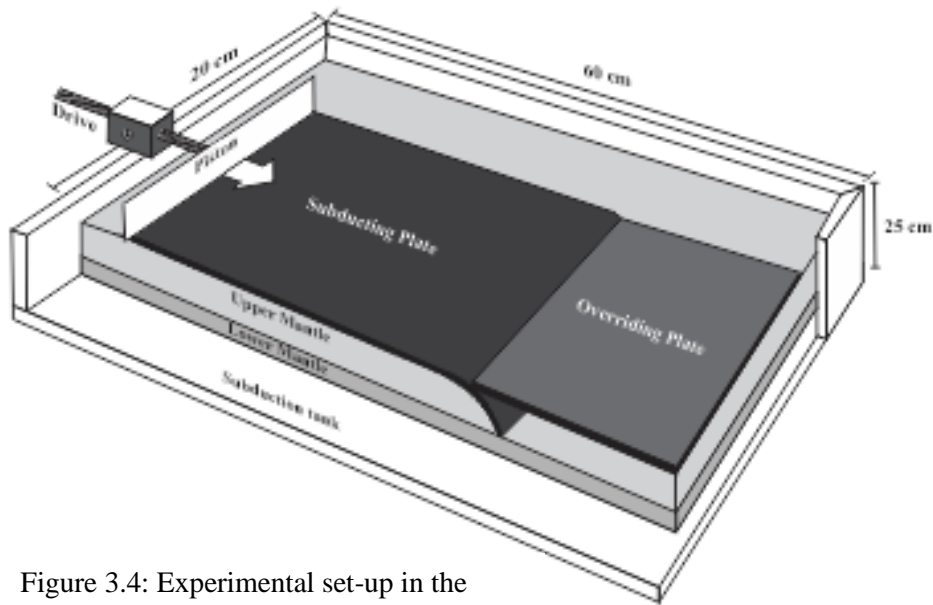


Figure 3.4: Experimental set-up in the laboratory.

The above diagram shows a schematic diagram of the set-up of the experiment carried out in the laboratory. It consists of a rectangular glass box having dimensions 60cm*20cm*25cm. It is provided with an indenter at its side to induce pull-push action, ie, to produce a zone of compression and extension. For our convenience, mantle structure has been divided into two parts- one, more viscous lower mantle which is simulated using high viscosity glucose syrup and another, less viscous upper mantle which is modelled using low viscosity glucose syrup. Subducting lithospheric plates are imitated using plasticine material which has a visco-elastic property alike the lithosphere. Apart from that, there were weak zones which were modelled using PDMS (Poly Dimethyl Siloxane) and hand putty.

3.5. Physical Variables

In the laboratory set-up, certain experimental parameters were taken into account.

- (1) *Geometry*- It is an important aspect which accounts for the shape and size of the subducting plate. Apart from this, the structure of the subducting slab (homogeneous or inhomogeneous) provides great influence on the mode of deformation acting on the slab. Subduction experiments were performed with both of these structures which infer variability in deformation mode with due course of evolution.
- (2) *Kinematics*- This parameter accounts for the convergence of the subducting slab. It has been a topic of debate on what controls the kinematics of subduction (pull or push or both). For the laboratory experiments most of them were self-sufficient subduction governed by the negative buoyancy of the slab, created by pre-defined density differences. However, a constant push by the indenter was exerted on the slab in some cases to replicate the ridge push force.
- (3) *Mechanical properties*- It accounts for the mechanical strength of the modelling materials representing the subducting slab domains. For, the experiments, the mechanical strength of the weak-zone was varied in such a way that yield strength of the material under deformation becomes different.

3.6. Type of Experiments

In order to understand the conditions of subduction, two types of experiments were conducted, taking into account the variable physical conditions and heterogeneity of lithospheric slab.

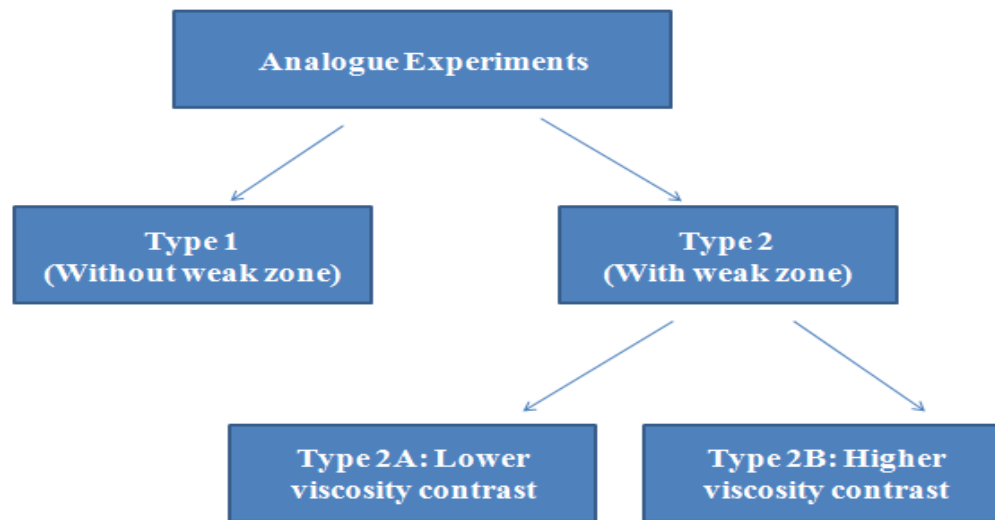


Figure 3.5: Types of experiments.

Type 1: In this set of experiment, the subducting lithosphere was modelled using pure plasticine. In this setup, the slab has been kept homogeneous, without the interference of any other material. This was done to investigate the behaviour of a slab in the absence of any weak zone.

Type 2: Here, in this category, the lithospheric slab made of plasticine was coupled with a layer different from the slab material, marking the weak zone. Two types of materials were used for simulating the weak zone, based on the viscosity contrast between the slab material and the material of the weak zone. Type 2A experiments were conducting using a weak zone made up of

low viscosity contrast PDMS(Poly Dimethyl Siloxane) whereas, Type 2B experiments were carried out with higher viscosity contrast hand putty.

CHAPTER 4:

SUBDUCTION ZONES AND ANALOGUE MODELS

4.1 General Description

The geometry, slab dip and curvature are dependent on the dynamics of subduction and the mantle flow underneath it. Apart from that, there are other forces which act on a descending slab. One such example is the relative velocity between the two converging slabs. Negative buoyancy which arises from the high density oceanic plate also guides the nature of subducting plate. At the mantle transition zone (~660 km), where there is a phase transformation between olivine and spinel, the effect of negative buoyancy or slab pull gets modified (*Tokanobu Yokokura, 1981*). These presumptions are applied in the laboratory modelling. The subduction is assisted by negative buoyancy of the slab material due to pre-defined density variation. The model is scaled in such a way with the nature that the bottom surface of the model represents impermeable transition zone (660 km). The convergence motion is created by coupled effects of negative slab pull force and ridge push force exerted by the moving indenter.

4.1.2 Experiment Type 1

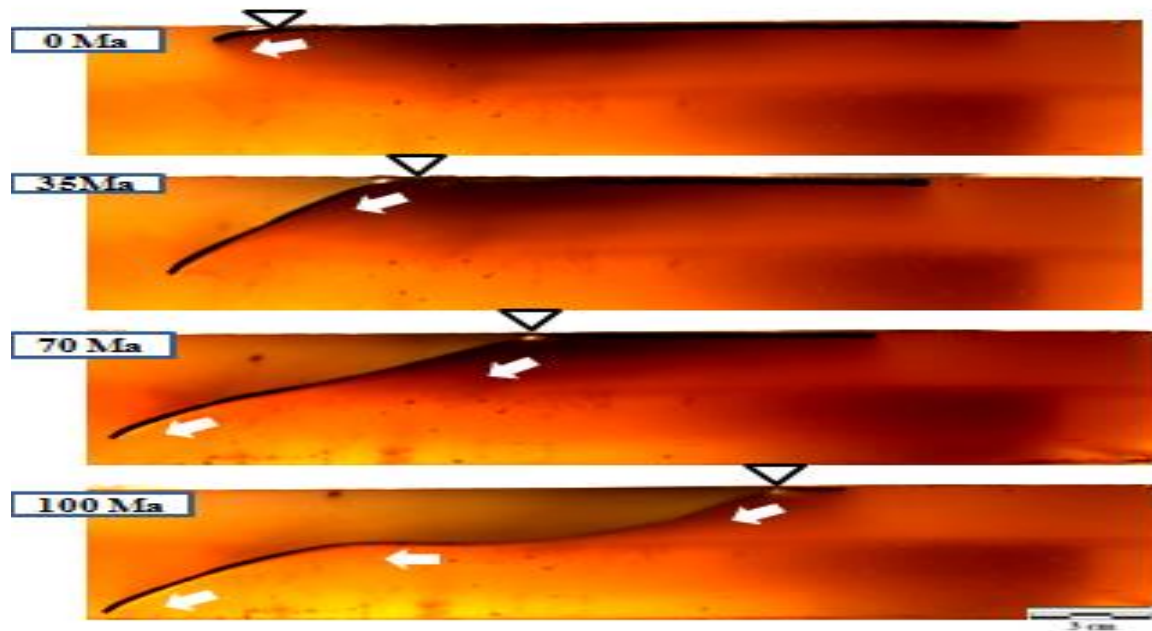


Figure 4.1: Evolution of a pure plasticine slab.

In this set of work, experiments were conducted taking homogeneous subducting slab. This is introduced by pure plasticine as the modelling material for lithospheric slab. Plasticine behaves as visco-elastic material and I have made use of this particular property. As the subduction begins, the slab dip increases and the horizontal plate movement is very less. After some period, the subducting slab dip increases with greater rate while the slab reaches a stable state. Finally, when the slab attains its ultimate stage, the rate of increase in dip becomes less rapid. So, overall, there is an increase in dip amount with the progression of time. The point of subduction shifts during each time step as the trench retreats and the subducting slab length increases in due course of subduction. There was also a considerable change in the radius of curvature of the subducting slab. It is observed with the gradual increment in time, the slab curvature keeps on decreasing, thus resulting slab steepening.

4.1.3 Experiment Type 2

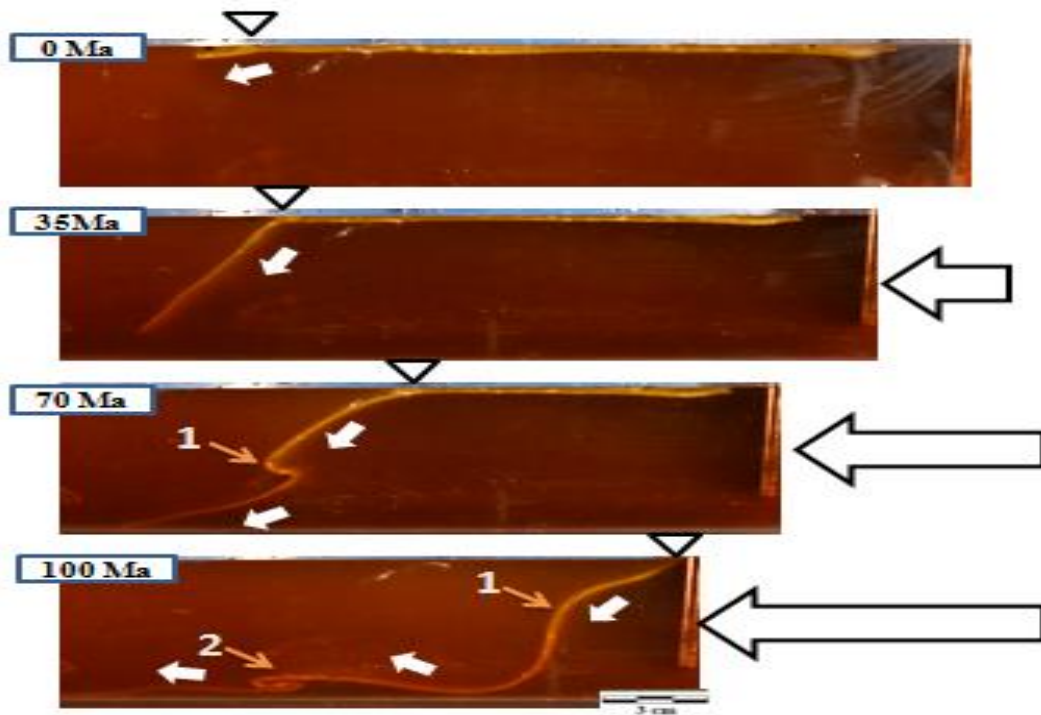


Figure 4.2: Evolution of a slab with weak zone of PDMS.

In this experiment, a trench parallel weak zone was introduced in the plasticine slab with PDMS (Poly Dimethyl Siloxane) which turned the slab into a heterogeneous one. PDMS is a material which has a low viscosity contrast with respect to the adjoining plasticine slab. Thus, along the length of the plasticine material, there now appears a weak zone which is simulated using PDMS. In nature, weak zones result from thermal induction or presence of dead ridges. The set up was provided with an indenter which applied a compressive force, parallel to the slab. As the experiment initiated, there is an increase in subducting dip of the plate. However, at a certain time, with increase in force exerted by the indenter, the slab showed folds of buckling

nature, at the junction of weak zone. With the appearance of these folds, there occurs a reduction in slab dip, after which the dip again started increasing. The part of the slab sunk into the mantle, was already undergoing deformation, so, after a certain time interval, there developed a second order folding. At this point of time, the slab dip again decreased, soon after which, it again started to increase. Also, with the progression of time, though the slab undergoes folding, there is a systematic reduction in the radius of curvature.

4.2 Subduction Dip Analysis

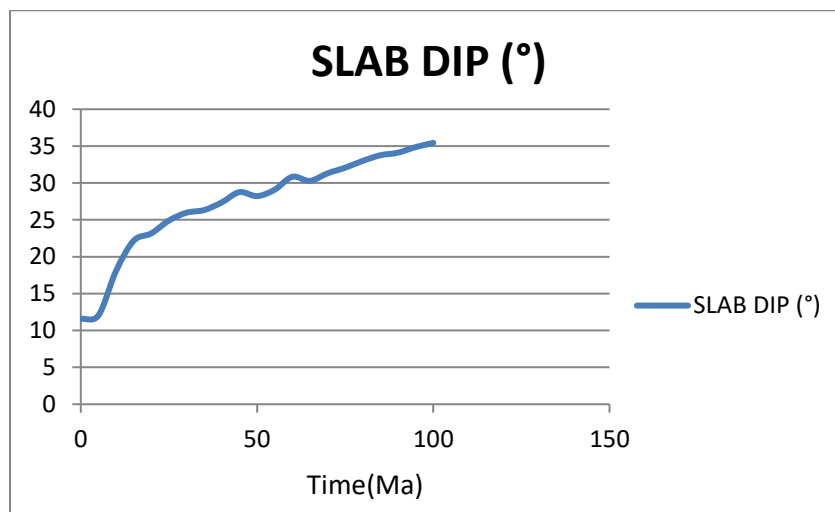


Figure 4.3: Curve representing the evolution of dip for a pure plasticine slab.

When pure plasticine was used for modelling the lithosphere, the subduction dip keeps on increasing. This was in tune with the increasing slab pull with time, as compared to the ridge push. Initially, at 0 Ma, the slab dip was 11.57° , which increased to 24.91° at 25 Ma. From that point, the slab dip increased but it was gradual. At 60 Ma, the slab dip was 30.84° . When time was 90 Ma, the dip changed to 34.11° . Ultimately, in the final step of 100 Ma, the slab dip became 35.44° .

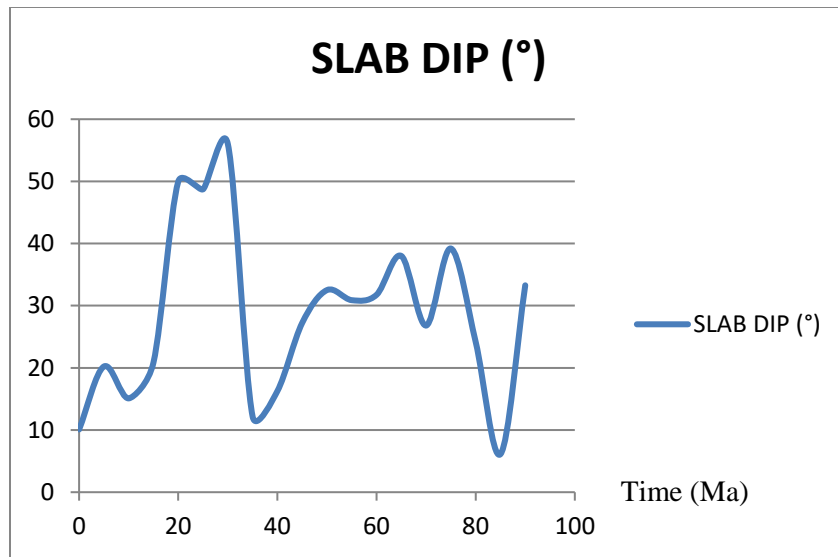


Figure 4.4: Curve representing the evolution of dip for a pure plasticine slab.

When plasticine was combined with PDMS weak zone, we find there was a periodic rise and fall in dip amount. This decrease in dip accounted for the folding of the slab when encountered with a layer parallel compression. In this case, the ridge push offered by the mid-oceanic ridge is very dominant which causes the slab to buckle. The slab dip naturally decreases with subsequent folding. In case of this experiment, the slab dip initially was 10.09° . With the increment in time, at 30 Ma, the slab dip was 56.02° , soon after which at the next step it dropped down to 12.17° , indicating a folding activity. Then, there was a general rise in dip from 40 Ma to 65 Ma, i.e., from 16.27° to 26.15° . However, since at 70 Ma, the slab encountered another order of folding, so there was a fall in dip value to 25.62° . However, at the final step the slab dip remains 33.28° .

4.3 Subducting Plate Curvature

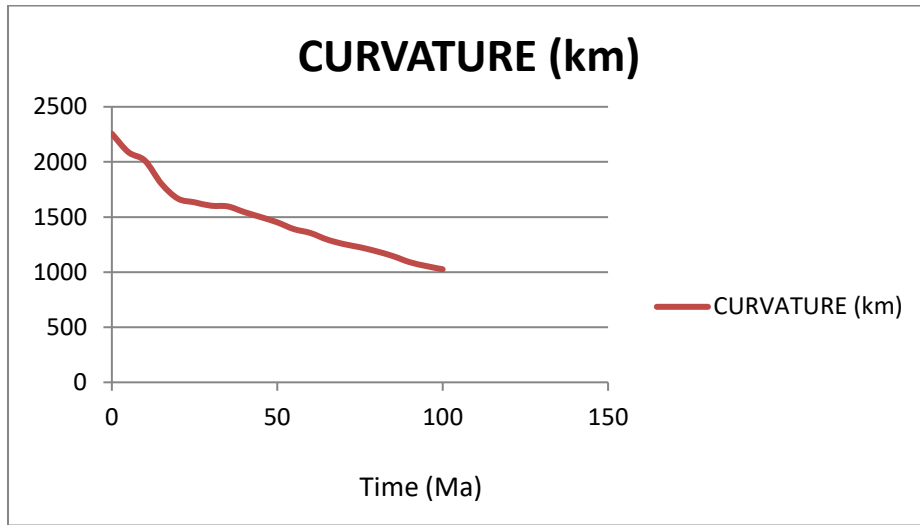


Figure 4.5: Evolution of curvature of a slab with pure plasticine.

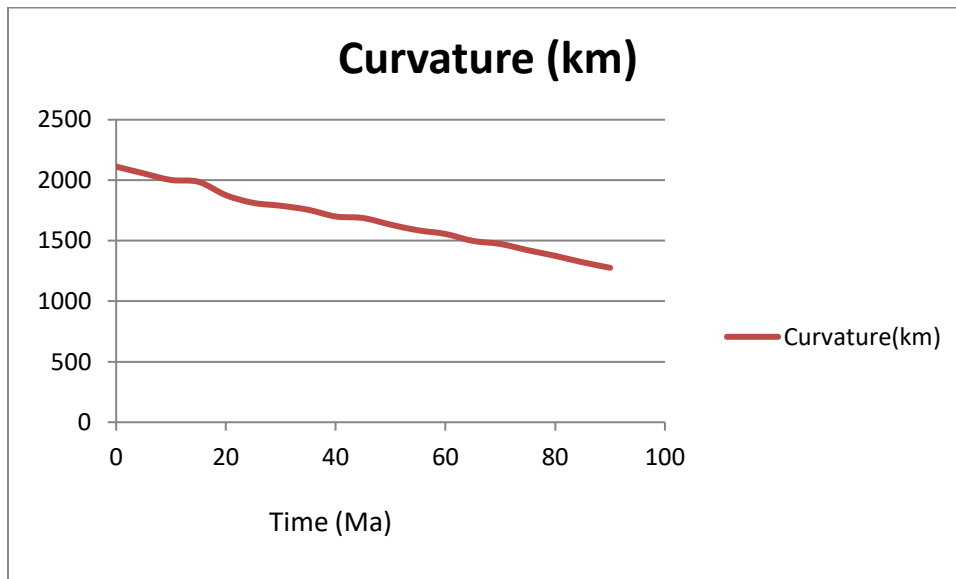


Figure 4.6: Evolution of curvature of a slab with plasticine combined with PDMS.

With the onset of subduction, there occurs a decrease in slab curvature, irrespective of the material of the slab. In both the cases, be it pure plasticine or with the combination of PDMS, the slab dip decreases. This points out to an overall steepening of the slab. In case of first graph, the radius of curvature constantly decreases with time. Initially, it was 2256 km, at 30 Ma it is 1602.5 km, at 70 Ma it is 1255.17 km and at 100 Ma, it is 1025.5 km. Similarly, for the second graph, initially the slab radius was 2112.5 km, then it changed to 1788.99 km at 30 Ma, 1473.21 km at 70 Ma and finally, at 90 Ma it became 1276.24 km.

4.4 Subducting Slab Detachment

Slab breakoff is generally associated with continental subduction (*Dewey and Bird, 1970; McKenzie, 1969*). When positively buoyant continental lithosphere enters a subduction zone, down-dip tensile stress is generated in the previously subducted oceanic lithosphere,*2012*; which can lead eventually to slab breakoff (e.g. *Burkett and Gurnis, 2012; Burkett and Billen, 2009, 2010; Chemenda et al., 1996; Davies and von Blanckenburg, 1995; Duretz et al., 2011, 2014*). Slab detachment is initiated with the presence of a weak zone in any point on the the lithospheric plate. With the gradual progression of time, as the slab subducts below the mantle, the weak zone get more strained, resulting in partial or complete rupture from the original slab. This phenomenon is replicated in the laboratory with the help of plasticine slab which is coupled with a weak zone of hand putty. Hand putty has a high viscosity contrast with respect to the plasticine slab. This particular property is exploited to understand the change in slab dip as well as slab curvature. It also gives an account of the geometry of the plate.

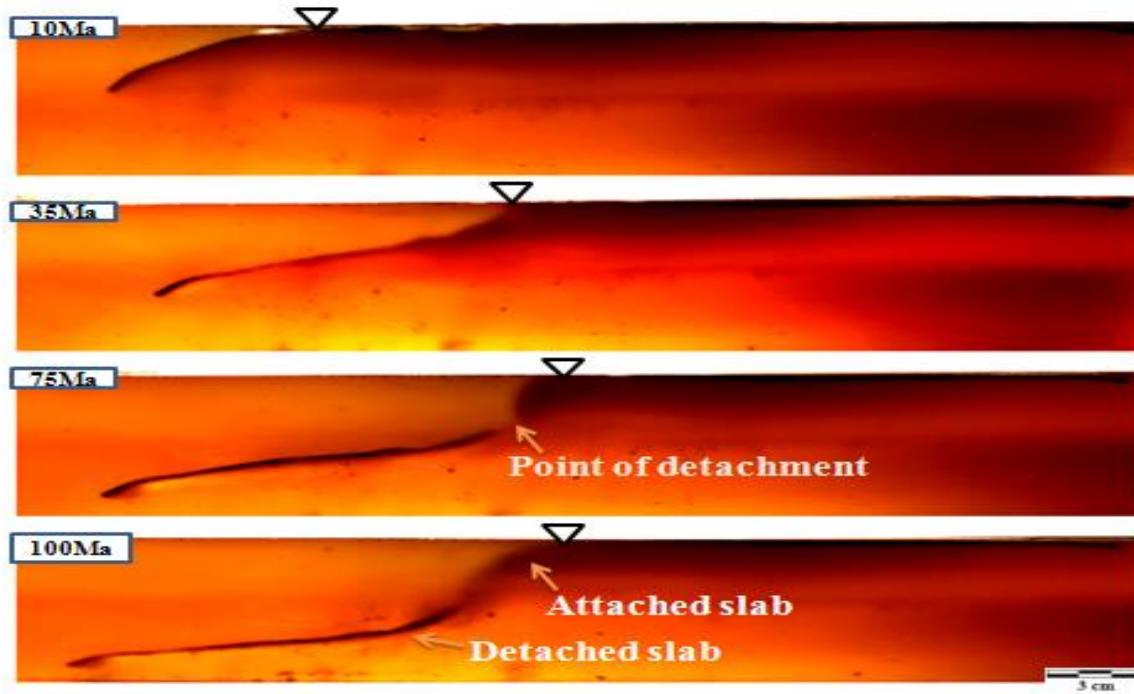


Figure 4.7: Evolution of a slab undergoing detachment.

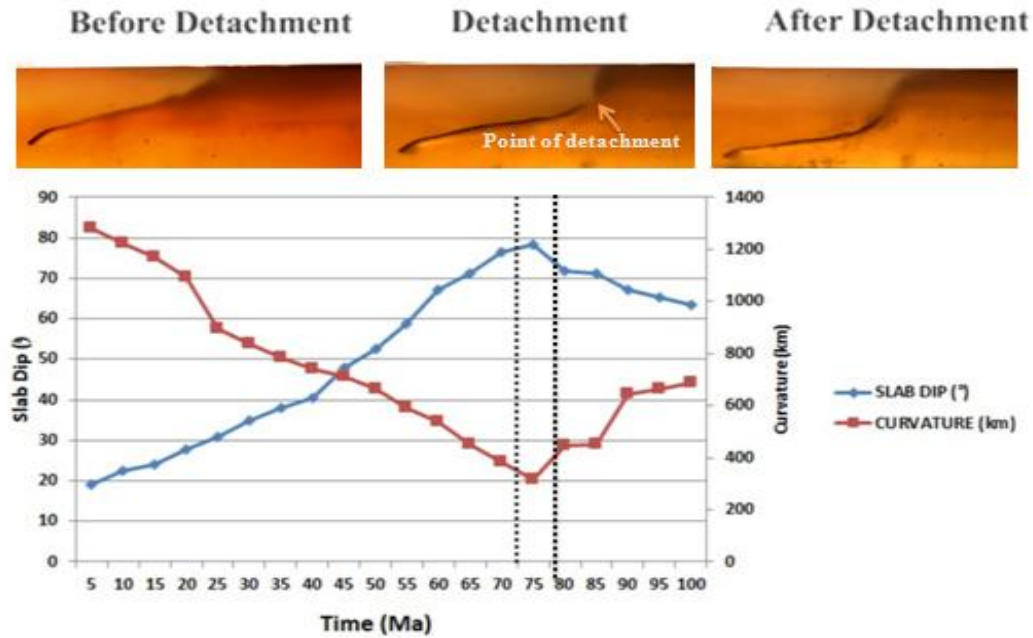


Figure 4.8: Evolution of slab dip and curvature with time.

At the slab sinks into the mantle, the slab dip starts increasing whereas, the radius of curvature starts decreasing. After this the slab detaches from the original slab and the event of subduction continues for a certain time interval. Soon after detachment is over, the dip starts decreases whereas the radius of curvature is enhanced. This mainly occurs due to cut-off of the slab pull force.

Initially, the slab dip at 5 Ma was 19.13° and the curvature was 1280.5 km. From this point, the dip increases to 78.45° and radius decreases to 313.5 km at 75 Ma. After this occurs the event of slab detachment and right after which the there occurs a reversal in the trend of the curvature as well as the dip. From 80 to 100 Ma, the dip changes from 71.67° to 63.32° while, the radius increases from 443.83 km to 687.17 km.

4.5 Deformed Slab Geometry

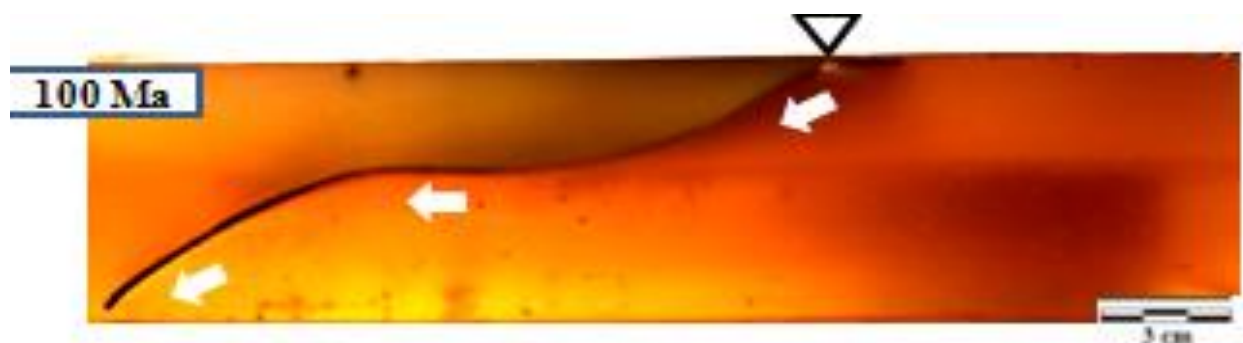


Figure 4.9: Geometry of pure plasticine slab (Type 1)



Figure 4.10: Geometry of plasticine slab coupled with PDMS weak zone.
(Type 2A)

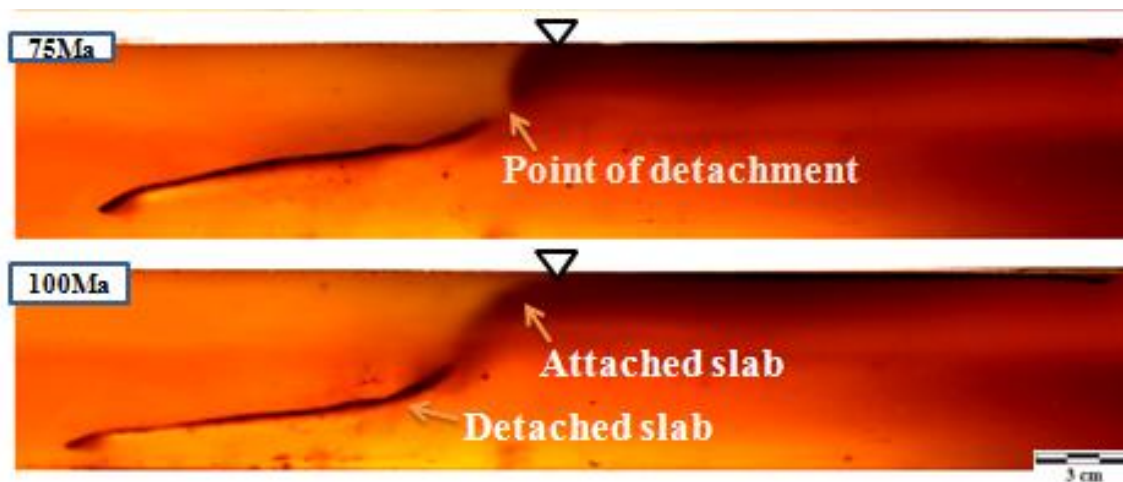


Figure 4.11: Geometry of plasticine slab coupled with hand putty weak zone. (Type 2B)

The geometry of a subducting plate is a guiding factor towards the reaction of stress to the plate. It changes from one setting to another setting and also the on the existence of a weak zone. Type 1 comprising of pure plasticine, with gradual time step shows bending nature. Here, the forces work perpendicular to the slab, with the ridge push dominating in intensity. Type 2 experiments were conducted with plasticine that is combined with a weak zone. For modelling these weak zones, two types of materials were used- PDMS (Poly Dimethyl Siloxane) and hand putty. For

Experiment Type 2A where weak zone of PDMS was used, the slab geometry showed sequence of folding. Buckling folds of generation 1 and 2 developed due to the application of compressive force in the form of indenter motion. However, the response of geometry changed when we replaced the PDMS with hand putty. The slab showed partial to complete detachment. The detachment of the slab is a continuous process as revealed from the Type 2B experiments. Due to interaction between pull and push force and slab-transition zone, deformation localizes in the introduced incompetent weak-zone of the subducting slab. The weak-zone gets stretched and necked and ultimately it gets detached from the slab complex. As a result of removal of negative buoyancy in form of detachment, the undetached portion experiences reduction of slab dip as a response.

CHAPTER 5:

THEORY OF FLUID DYNAMIC SIMULATION

5.1. Rheological Considerations and Governing Equation

A range of rheological classes have been considered in subduction modeling. Several workers have used Maxwell type visco-elastic rheology to study lithospheric processes, such as slab bending and their effects on topography (*Melosh and Rafeesky, 1980; Gurnis et al., 1996, Kumar et al., 2010*), and the dynamics of subduction initiation (*e.g., Toth and Gurnis, 1998; Regenauer-Lieb et al., 2001; Hall et al., 2003 ; Nikolaeva et al., 2011*). However, majority of the current studies employ fluid models with either power-law (*Schmeling et al., 2008; Holt et al., 2015*) or linear viscous (*Manea et al., 2007*) rheology providing a good rheological approximation to large-scale geodynamic settings on long time scales (million years) (*McKenzie et al., 2000*). In this study I have used linear viscous rheology to develop the subduction model (Figure 3.). The viscous fluids are assumed to be incompressible, and their rheological equations follow,

$$\sigma_{ij} = -p\delta_{ij} + 2\mu\epsilon_{ij}, \quad (1)$$

where σ_{ij} and ϵ_{ij} are the stress and the strain rate tensors, respectively, δ_{ij} is Kronecker delta, p is the hydrostatic pressure, and μ is the co-efficient of viscosity of fluid. In our simulation, we consider iso-viscous rheological model for the lithosphere ($\mu \sim 10^{22}$ Pa s), whereas stratified viscous structure for mantle with the viscosity ranging from $\sim 10^{20}$ to 10^{21} Pa s (details discussed later).

The computational fluid dynamics (CFD) simulations operate fundamentally on the two governing equations based on: conservation of mass and momentum. The continuity equation balances the change of mass with time inside an elemental volume being equal to the net flow of mass into or out of the volumes,

$$\frac{\partial \rho}{\partial t} + \nabla \cdot (\rho \mathbf{u}) = 0, \quad (2)$$

Where ρ is the density and \mathbf{u} is the velocity vector of fluid flow. The conservation of momentum equation for a viscous medium (Navier-Stokes equation) represents a balance of the following forces: inertial, viscous and pressure forces, and body forces due to gravity,

$$\rho \frac{\partial \mathbf{u}}{\partial t} + \rho (\mathbf{u} \cdot \nabla) \mathbf{u} = \nabla \cdot [-p\mathbf{I} + \boldsymbol{\tau}] + \mathbf{F}, \quad (3)$$

Where p is the hydrostatic pressure, \mathbf{I} and $\boldsymbol{\tau}$ are the unit and viscous stress tensors, respectively. The last term, \mathbf{F} on the right side represents the body force per unit volume. In the present case the inertial term is neglected ($\rho \frac{\partial \mathbf{u}}{\partial t} = 0$) as the mantle flow is an extremely slow process, operating on a time scale of million years. The Navier-Stokes equation thus simplifies to

$$\rho (\mathbf{u} \cdot \nabla) \mathbf{u} = \nabla \cdot [-p\mathbf{I} + \boldsymbol{\tau}] + \mathbf{F} \quad (4)$$

Since our model deals with a large-scale fluid system, the effects of surface tension can be ignored.

The viscous stress tensor term is then expressed as,

$$\boldsymbol{\tau} = \mu \mathbf{D}, \quad (5)$$

Where \mathbf{D} is the strain rate tensor, $\mathbf{D} = [\nabla \cdot \mathbf{u} + (\nabla \cdot \mathbf{u})^T]$

5.2. Numerical Scheme

We use the well-recognized Two-phase flow Level-set method for implementing the governing equations. This is an implicit method for capturing the evolution of an interface. In our case I have considered the lithospheric slabs as one phase and the underlying mantle as another phase. Consider a simple closed curved $\Gamma(t)$ in a two-dimensional space to define the interface between the two fluids phases, attributed to a velocity field, $\mathbf{v} = (v_x, v_y)$. A level set (LS) function φ is chosen, where the zero-level set ($\varphi = 0$) detects the evolving interface $\Gamma(t)$. The LS function is restricted to a domain as,

$$\varphi = \varphi(r, t), \quad r \in \Omega, \quad (6)$$

where, Ω is the domain of interest, defined by the physical problem. The time dependent expression of φ corresponding to the moving interface is given by the advection equation,

$$\partial_t \varphi = \mathbf{v} \cdot \nabla \varphi \quad (7)$$

Considering the two fluids separated by the interface Γ in the domain Ω as incompressible, the velocity field must satisfy the divergence equation, $\nabla \cdot \mathbf{v} = 0$. Eq. (7) can be then written as

$$\partial_t \varphi + \nabla \cdot (\mathbf{v} \varphi) = 0 \quad (8)$$

This represents a continuity equation of the level set function.

The numerical approach approximates the solution to the time-dependent initial value problem of the associated level set function, where the zero-level set can always locate the moving interface at an instant. For a standard level set method, an indicator of the LS function φ is

defined as assigned distance to the interface Γ , and the smallest distance between a given point in the domain and the interface,

$$|\varphi(X, t = 0)| = \min_{X_\Gamma \in \Gamma} (|X - X_\Gamma|), \quad (9)$$

is used to delineate the interface. $\varphi > 0$ represents one side of the interface, whereas $\varphi < 0$ the other side, while the zero LS of φ indicates the interface:

$$\Gamma = \{X | \varphi(X, t) = 0\} \quad (10)$$

The conservative level set method, on the other hand, employs a Heaviside function as,

$$H(\varphi) = \begin{cases} 0, & \varphi < 0 \\ 1, & \varphi > 0 \end{cases} \quad (11)$$

However, an abrupt jump in the field, as defined by the Heaviside function in Eq. (11) causes instabilities in the computational operations, especially when the materials on either side of the interface have strong contrasts in their physical properties. To overcome this problem a smeared out Heaviside function is used in the conservative LS method in the form,

$$H(\varphi) = \begin{cases} 0, & \varphi < 0 \\ \frac{1}{2} + \frac{\varphi}{2\varepsilon} + \frac{1}{2\pi} \sin\left(\frac{\pi\varphi}{\varepsilon}\right), & -\varepsilon \leq \varphi \leq \varepsilon, \\ 1, & \varphi > 0 \end{cases} \quad (12)$$

Where ε denotes half the thickness of the interface. The interface thickness depends on the grid size chosen for meshing. We can now define a new LS function,

$$\Phi(r) = H_{sm}(\varphi(r)) \quad (13)$$

The LS function in Eq. (8) has an advantage in the sense that the function describes continuous variations of the material properties across the interface. For example, the density and the viscosity of the two fluids can be expressed as,

$$\rho(r) = \rho_1 + (\rho_2 - \rho_1)\Phi(r), \quad (14)$$

$$\mu(r) = \mu_1 + (\mu_2 - \mu_1)\Phi(r), \quad (15)$$

Where ρ_i and μ_i are the density and the viscosity of phases, $i = 1, 2$. The interface is attributed to the 1/2-level set, as defined in Eq. (13). While operating with interfaces it is necessary to define the normal vector and the curvature of the interface, which are obtained from the distance function,

$$\mathbf{n} = \frac{\nabla\varphi}{|\nabla\varphi|} \quad (16)$$

$$\kappa(\varphi) = -\nabla \cdot \mathbf{n} = -\nabla \cdot \frac{\nabla\varphi}{|\nabla\varphi|} \quad (17)$$

It is noteworthy that the shape of φ can be complexly distorted due to a strongly heterogeneous velocity field, leading to inevitable numerical errors or artificial diffusion and the numerical problem can turn worse. To overcome this hurdle, Olsson et al. added an a re-initialization step to maintain the shape and width of the interface by using the following equation,

$$\partial_t\varphi + \nabla \cdot \left(\frac{\varphi(1-\varphi)\nabla\varphi}{|\nabla\varphi|} \right) = \nabla \cdot (\varepsilon(\nabla\varphi \cdot \mathbf{n})\mathbf{n}) \quad (18)$$

In Eq. (13), the diffusion in the normal direction is balanced by the compressive term, where the shape and the width of the interface are conserved. These interface conditions are compulsory in order to maintain the conservative properties of the interface.

CHAPTER 6:

SUBDUCTION ZONES IN NUMERICAL MODES

Numerical modeling following different schemes (finite element, finite difference, boundary element, discrete element), have been exhaustively used for simulating subduction zones. There are various challenges for modeling a subduction zone.

Firstly, for a real scale simulation, the extent of model domain is very large as subduction of lithospheric slab is a tectonic scale phenomenon. In addition, to accommodate large amount of deformation within this work frame is also an issue. To overcome this I have applied mapped triangular mesh throughout the model, which enables solvers like MUMPS (MULTifrontal Massively Parallel Sparse direct Solver) calculating precise solutions on each nodal point of the meshes while converging the whole time dependent study.

Moreover, due to large geometrical extent, the model domain inherits rheological heterogeneity both in the length and depth direction. I incorporated this heterogeneity in the model by using step functions instead of introducing multiple domains.

Finally, as my subduction model is of real scale with large run time (at least 50 Ma), it involves huge computational resources. All the experiments were performed in a Cluster computer hosted in High Pressure Temperature Laboratory, Jadavpur University.

The numerical simulation of subduction zone was performed using the Finite Element Package COMSOL Multiphysics version 5.3. The numerical scheme used to track the deformation of subducting slabs is governed by Two-phase Level Set method. A detailed discussion of the numerical technique and scheme are manifested in Chapter 5.

6.1. Model Setup

The lateral extent of the model is 6000 km and the vertical extent is of 1600 km. It consists of two lithospheric slabs each 3000 km long and 100 km. thick. The subduction has been initiated by protruding a small frontal part of the subducting slab in the mantle. Long wavelength analysis and Monte Carlo simulation of geoid data suggests that the lower mantle is 10 times more viscous than the upper one. Incorporate this viscosity jump in the mid-mantle at around 660 km by introducing a step functions, smoothed up to second order derivative level. The viscosity of the upper mantle (10^{20} Pa.s) gets multiplied ten times in the lower mantle (10^{21} Pa.s). There is a low viscosity channel (5×10^{19} Pa.s) sandwiched between the upper and lower mantle. The density and viscosity of the over-riding slab is considered as 3200 kg/m^3 and 10^{22} Pa.s respectively, which closely resembles the property of a continental slab. The density and viscosity of the subducting slab was varied considering different ages. To evaluate the age dependency on lithospheric rheology, “Half space cooling model” was used to predict the rheological parameters like density and viscosity. Although, rheology is variable along the depth for a specific aged slab, but for simplification, we computed an average viscosity and density value for each age range. The computation of half space-cooling model was done using temperature dependent density and non-linear power law rheology as proposed by previous workers (*Hirth and Kohlstedt*). For avoiding error during rheological approximation, an age range was taken instead of a fixed age value corresponding to a specific rheology. By varying density and viscosity of the subducting slabs,

which is the representative for different ages (younger to older) subduction zone modeling was done to see the difference in their subduction dynamics. From the calculation, a 10, 60 and 100 Ma old slab is considered to have density values of 3240, 3260 and 3280 kg/m^3 , respectively. The upper and lower mantle have density values of 2900 and 3100 kg/m^3 , respectively.

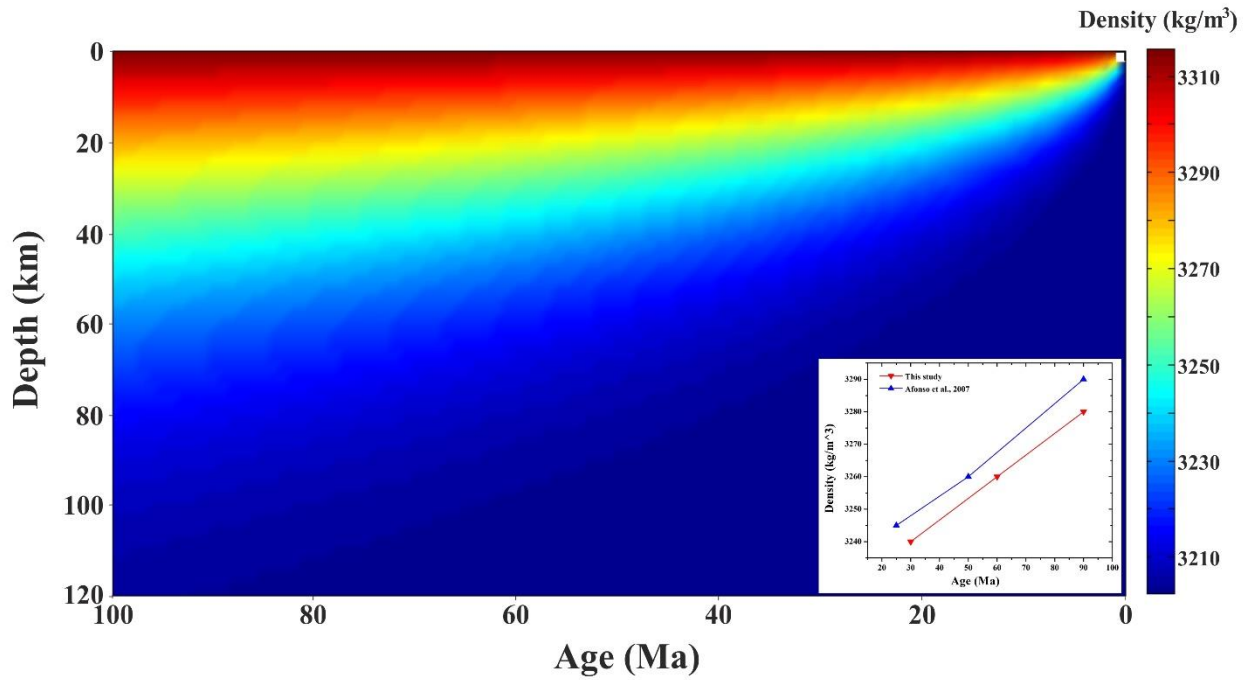


Figure 6.1: Estimation of average density of the lithosphere of different ages from the half-space cooling model [*Turcotte and Schubert, 2014*]. A regression diagram of change in density with age used in this study and (*Afonso et al., 2007*) are shown in the inset.

6.2. Boundary Conditions

The boundary conditions for the modeling are shown in figure X. The bottom boundary is considered as a no slip one. The lateral boundaries are free slip. A velocity of 4 cm/year on the upper boundary of the subducting slab. However, for over-riding slab the upper boundary is left unconstrained for it to move and deform solely upon the interaction and influence of the subducting slab. For the slab detachment, paucity in convergence velocity is introduced, as it enhances the interaction between ridge push and slab pull forces in the subducting slab. For 100 Ma of model run time, a constant convergence velocity of 4 cm/yr is assigned for 40 Ma and for rest 60 Ma there is no convergence velocity. As mentioned earlier a shallow initial dip is introduced for the subducting slab as the subduction has already begun and the study does not aim to model the initiation of subduction. I have run all the models for 100 Ma though it reaches the transition zone much before than that.

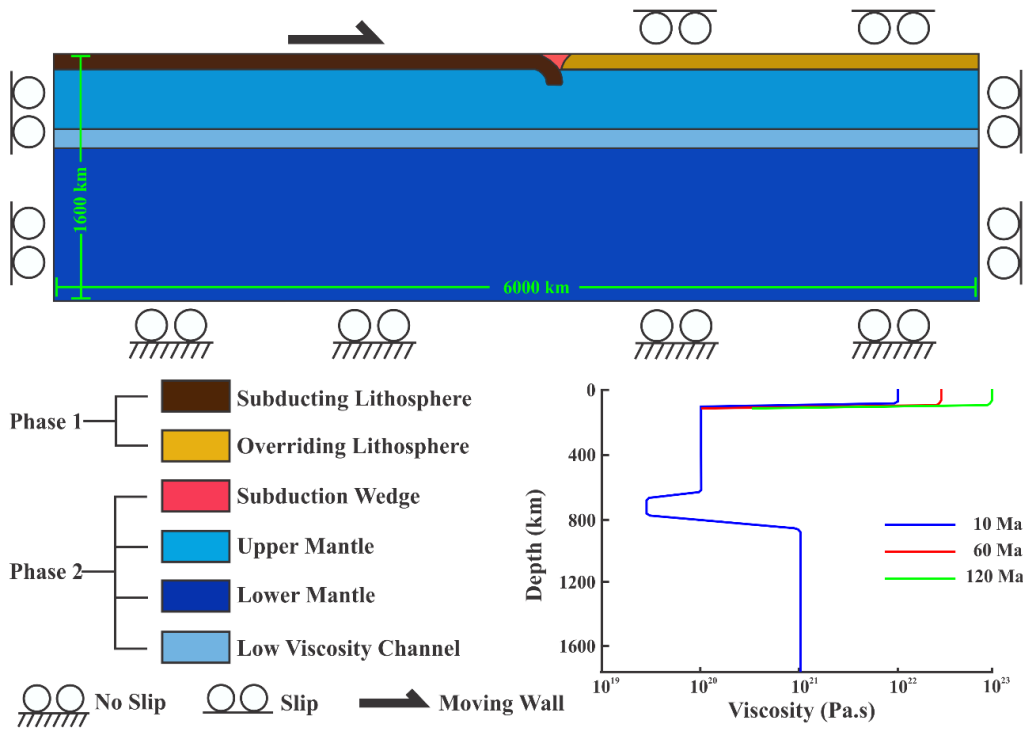


Figure 6.2: The geometry of the numerical experiment. Different domains of the model are marked in color and indexed at the bottom panel. The Subducting and Overriding lithospheres are considered as Phase 1 and the whole mantle as Phase 2. The boundary conditions assigned in different boundaries of the model domain are also indexed. The graphical plot shows change in the vertical viscosity profile for three sets of experiments with slabs of different lithospheric ages.

6.3. Analysis of Plate Geometry

Three types of numerical experiments were conducted varying the age (in terms of viscosity and density) of the slabs. For Type 1 experiment, the 10 Ma old subducting slab possess 3240 kg/m^3 density and 10^{22} Pa.s viscosity. The slab while encountering the transition zone yields a radius of curvature of 890 km. The slab dip is 45° during 30 Ma while it attains a dip of 86° during 70 Ma. The dynamic subduction pattern for the Type 1 numerical experiment is similar to the laboratory model (Figure 3). With progressive time steps the slab dip increases gradually before penetrating the transition zone. During the interaction of subducting slab with the upper-lower mantle boundary, the slab shows little to no deflection. For Type 2A experiment, 60 Ma old subducting slab (3260 kg/m^3 density and $5 \times 10^{22} \text{ Pa.s}$ viscosity) was considered. The slab interacts with the transition zone at about 80 Ma though it does not penetrate it. The slab shows a radius of curvature of 620 km during model run time of 70 Ma, before interacting with the upper and lower mantle boundary. It shows typical hook like folded geometry over the transition zone. The slab shows profuse folding and refolding near the transition zone. At initial stages (10 Ma) the subducting slab exhibits a shallow dip of 27° which increases to 80° . Like laboratory experiments, periodic change is also observed in each slab folding stage.

Lastly for Type 2B experiments old (100 Ma) slabs possessing density value of 3280 kg/m^3 and viscosity value of 10^{23} Pa.s was used. The initial (10 Ma) dip of the slab was 45° which increased to 73° within 30 Ma of model run time. The detachment due to the combine effect of paucity in convergence rate and high negative buoyancy takes place during 70 Ma. Strikingly the slab dip reduces to 54° after the detachment due to reduction of negative slab pull. The detached portion ceases to act in the cumulative negative buoyancy budget which reduces the slab dip. At

the time of detachment the slab radius of curvature becomes 458 km. After detachment, the separated slab becomes stagnant in the 660 km transition zone.

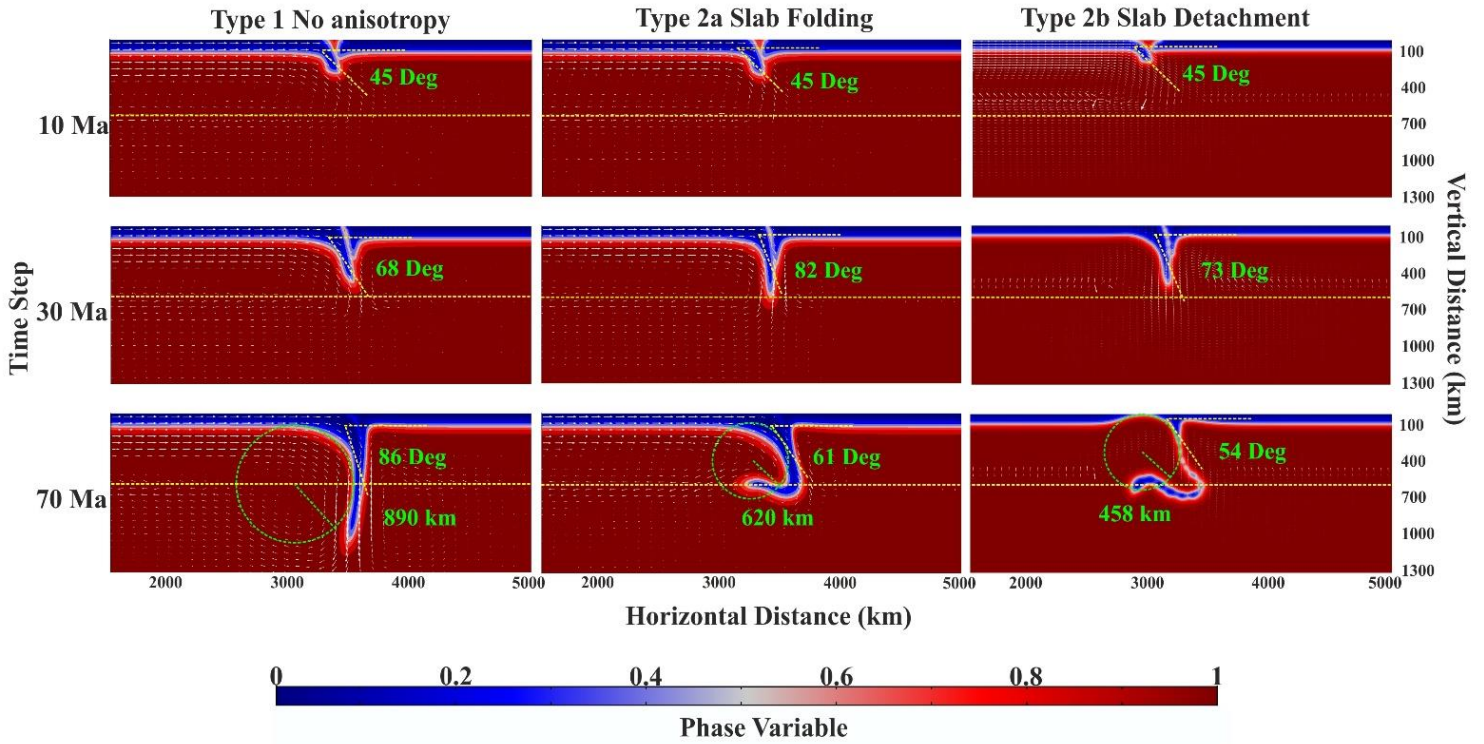


Figure 6.3: Results of three sets of numerical experiments. The blue color represents Phase 1 and the red one Phase 2. Evolution of dip at each stages for all the experiments are denoted. A time dependent evolution consisting representations of deformed subducting slab geometry at 10, 30 and 70 Ma are represented vertically for each type of experiments.

CHAPTER 7:

SUMMARY AND CONCLUSIONS

The following conclusions can be drawn from this study:

(1) Trench retreat versus subducting slab geometry

The slab geometry changes with the retreat of trench position. With time the dip of the slab increases as the trench retreats. However, when the slab interacts with the transition zone (660 km) the trench retreat phenomenon gets halted and it gets manifested in slab dip.

(2) Localized folding of subducting slab

Folding in the subducting slab is localized in the introduced weak zone. In course of subduction, during the interaction of the slab with the transition zone the folding starts to occur. This compressional deformation localizing in the weak zone gets enhanced due to coupled effect of ridge push and hindrance of slab motion by transition zone.

(3) Condition of slab detachment

Slab detachment takes place when the deformation of the subducting slab exceeds its yield strength. Large negative buoyancy of the slab, thermal weakening in the deformed zone and pre-existing weak zones in the subducting slab enhances the probability for detachment. However, the experiments reveal that low viscous incompetent weak zone

favours slab detachment. Also, a criticality in the negative buoyancy of the slab and a paucity in the convergence rate is crucial for slab detachment to take place.

(4) Change in slab dip with deformation

For all the experiments, during steady state of subduction the slab dip increases with time, resulting in slab steepening. However, slab deformation induces modification in the slab dip. Slab folding causes periodic decrease and increase in slab dip. Also, there is slab dip reduction right after detachment, due to sudden decrease in slab pull force as the detached portion ceases to contribute to the cumulative pull force.

(5) Subducting plate curvature at the trenches

Most of the experiments exhibit decrease in curvature with time during steady state of subduction. However, when slab detachment takes place, as the slab dip decreases the radius of curvature increases to maintain geometrical asperity.

REFERENCES

- Boutelier, D., & Cruden, A. R. (2017). Slab breakoff: Insights from 3D thermo-mechanical analogue modelling experiments. *Tectonophysics*, 694, 197-213.
- Capitanio, F. A., & Morra, G. (2012). The bending mechanics in a dynamic subduction system: Constraints from numerical modelling and global compilation analysis. *Tectonophysics*, 522, 224-234.
- Duretz, T., Schmalholz, S. M., & Gerya, T. V. (2012). Dynamics of slab detachment. *Geochemistry, Geophysics, Geosystems*, 13(3).
- Duretz, T., Gerya, T. V., & May, D. A. (2011). Numerical modelling of spontaneous slab breakoff and subsequent topographic response. *Tectonophysics*, 502(1-2), 244-256.
- Duretz, T., & Gerya, T. V. (2013). Slab detachment during continental collision: Influence of crustal rheology and interaction with lithospheric delamination. *Tectonophysics*, 602, 124-140.
- Duretz, T., Gerya, T. V., & Spakman, W. (2014). Slab detachment in laterally varying subduction zones: 3-D numerical modeling. *Geophysical Research Letters*, 41(6), 1951-1956.
- Guillaume, B., Martinod, J., & Espurt, N. (2009). Variations of slab dip and overriding plate tectonics during subduction: Insights from analogue modelling. *Tectonophysics*, 463(1-4), 167-174.

- Guillaume, B., Hertgen, S., Martinod, J., & Cerpa, N. G. (2018). Slab dip, surface tectonics: How and when do they change following an acceleration/slow down of the overriding plate?. *Tectonophysics*, 726, 110-120.
- Lee, C., & King, S. D. (2011). Dynamic buckling of subducting slabs reconciles geological and geophysical observations. *Earth and Planetary Science Letters*, 312(3-4), 360-370.
- Schellart, W. P. (2011). A subduction zone reference frame based on slab geometry and subduction partitioning of plate motion and trench migration. *Geophysical Research Letters*, 38(16).
- Stern, R. J. (2002). Subduction zones. *Reviews of geophysics*, 40(4), 3-1.
- Schellart, W. P. (2010). Evolution of subduction zone curvature and its dependence on the trench velocity and the slab to upper mantle viscosity ratio. *Journal of Geophysical Research: Solid Earth*, 115(B11).
- Stegman, D. R., Farrington, R., Capitanio, F. A., & Schellart, W. P. (2010). A regime diagram for subduction styles from 3-D numerical models of free subduction. *Tectonophysics*, 483(1-2), 29-45.
- Wortel, M. J. R., & Spakman, W. (2000). Subduction and slab detachment in the Mediterranean-Carpathian region. *Science*, 290(5498), 1910-1917.